Atmospheric convection as an unstable predator-prey process with memory

Maxime Colin, Steven Sherwood

Atmospheric convection as an unstable predator-prey process with memory

Maxime Colin*

(1) Climate Change Research Centre and ARC Centre of Excellence for Climate System Science, UNSW Sydney, Kensington, NSW, Australia

(2) Laboratoire de Météorologie Dynamique/IPSL, Sorbonne Université, Paris, France

(3) Laboratoire GEPASUD, University of French Polynesia, Punaauia, Tahiti, French Polynesia

Steven C. Sherwood

Climate Change Research Centre, UNSW Sydney, Kensington, NSW, Australia

Corresponding author: Maxime Colin, m.colin@unsw.edu.au OR m.colin@unswalumni.com OR [redacted]

Both authors contributed equally to this manuscript.

Early Online Release: This preliminary version has been accepted for publication in *Journal of the Atmospheric Sciences*, may be fully cited, and has been assigned DOI 10.1175/JAS-D-20-0337.1. The final typeset copyedited article will replace the EOR at the above DOI when it is published.

ABSTRACT

Heuristic models and observational analyses of atmospheric convection often assume that convective activity, for example rain rate, approaches some given value for any given large-scale ("macrostate") environmental conditions such as static stability and humidity. We present novel convection-resolving simulations in which the convective activity evolves in a fixed equilibrium mean state ("macrostate"). In this case convective activity is unstable, diverging quasi-exponentially away from equilibrium either to extreme or zero rain rate. Thus almost any rain rate can coexist with an equilibrium profile: the model rain rate also depends on convective history. We then present a two-variable, predator-prey model motivated by this behavior, wherein small-scale ("microstate") variability is produced by, but also promotes convective precipitation, while macrostate properties such as CAPE promote, but are consumed by convective precipitation. In this model, convection is influenced as much by its own history (via persistent microstate variability) as by its current environment. This model reproduces the simulated instability found above and could account for several lag relationships in simulated and observed convection, including its afternoon maximum over land and the well-known "quasi-equilibrium" balance at synoptic time scales between the forcing and response of key variables. These results point to a strong role for convective memory and suggests that basic strategies for observing, modeling and parameterizing convective processes should pay closer attention to persistent variability on scales smaller than that of the grid box.

Accepted for publication in *Journal of the Atmospheric Sciences*. DOI10.1175/JAS-D-20-0337.1.

Significance statement. To better predict weather and climate, it is necessary to better understand the process which creates cumulonimbus clouds and associated rainfall: atmospheric convection. Here, we suggest that convective inertia (so-called "convective memory") is a crucial aspect of convection.

We run a new type of cloud simulations, and detect an unsuspected kind of instability. To explain this, we introduce a predator-prey model of convection, in which the small-scale atmospheric structures are "hungry" for large-scale convective potential. The predator-prey model with memory recreates some typical convective phenomena. It is thus promising, and calls for more attention to small-scale processes.

The next question could be: how to put the right amount of memory, the right prey, and the right predator into climate models?

1. Introduction

The representation of atmospheric convection in global weather and climate models, via "parameterizations" or sub-models, is widely regarded as one of the main remaining challenges in global modeling (Arakawa 2004). The parameterization must predict the impact of unresolved convective processes at resolved scales. But, as in the more general case of fluid turbulence (Castelvecchi 2017), there is no comprehensive theory. Current parameterizations arguably have some solid foundations (Yano 2014; Yano and Plant 2016), but those in use still appear to produce inconsistent behavior (Hwong et al. 2021). Models can produce cloud and precipitation responses to warming that have opposite signs even in idealized settings (Stevens and Bony 2013) and show a wide range of extreme precipitation responses that seem related to model physics (Bador et al. 2018). As for convection in the present climate, models generally rain too often and too little (Stephens et al. 2010) and have difficulties with the diurnal cycle (Bechtold et al. 2014) and spatial organization

Accepted for publication in *Journal of the Atmospheric Sciences*. DOI10.1175/JAS-D-20-0337.1.

(Rowe and Houze 2015; Jiang et al. 2015). The entrainment rate of air into updrafts in "mass-flux" convection schemes (a commonly-used approach) tends to produce a better global-mean state if given a small value, but better variability if given a large value (Mapes and Neale 2011; Del Genio 2012). These issues suggest that a structural deficiency in these schemes cannot be ruled out. This situation motivates further exploration and testing of basic assumptions about convective behavior, particularly aspects that might be related to its organisation in space and time.

One common assumption about convection, here denoted the "diagnostic" assumption, is that grid-scale measures of smaller-scale convective activity (denoted C) at a given time and within a given region of size λ (O(100 km)) are determined only by the larger-scale environmental fields (denoted ξ) of that same time and region via some unknown function (f): $C(\mathbf{x}, t) = f(\xi(\mathbf{x}, t))$. This is explicitly assumed in simple theories of convectively coupled tropical disturbances (e.g. Raymond et al. 2015) and in traditional convective parameterization closures, for example that in the United States GFS weather forecast system (deriving from the classic scheme of Arakawa and Schubert (1974)). For a rich list of such diagnostic closures, see subsections 5b and 5c in Arakawa (2004); see Yano et al. (2013) for a review. This assumption is also implicit in observational studies that seek to empirically identify a general and instantaneous functional relationship between observed convective characteristics C and large-scale ξ from case studies (Jirak and Cotton 2007; Peters et al. 2013; Gottwald et al. 2016; Madonna et al. 2018; Sui et al. 2020). Imperfect prediction skill is sometimes addressed by including stochastic effects (Watson et al. 2015). The diagnostic assumption should not be confused with the so-called "quasi-equilibrium" assumption often discussed in the literature on convective schemes (Arakawa and Schubert 1974; Emanuel et al. 1994), which makes the more restrictive assumption that convection acts to balance the convective forcing, by keeping constant a control variable function of ξ (such as CAPE). Further

Accepted for publication in *Journal of the Atmospheric Sciences*. DOI10.1175/JAS-D-20-0337.1.

discussion of the diagnostic assumption can be found in Bougeault and Geleyn (1989); Arakawa (2004); Yano and Plant (2012c) and Colin et al. (2019).

The diagnostic assumption is expected to be valid as long as the scales involved are sufficiently large. But at small time and space scales (comparable to or smaller than those on which convection is organized), C could be directly affected by C at previous times or neighboring locations (for example via small-scale waves or density currents propagating long distances, or the persistence of turbulent motions which require substantial time to respond no matter how fast ξ might change). Recent studies have explored the limits of the diagnostic assumption, pointing out that "memory" of previous convective behavior can affect behavior at the current time t independently of $\xi(t)$ (Davies et al. 2009; Jones and Randall 2011; Davies et al. 2013; Colin et al. 2019; Daleu et al. 2020). Some modeling centers have added, or are now adding, prognostic variables to their parameterizations in an attempt to capture memory (Grandpeix and Lafore 2010; Park 2014; Willett and Whitall 2017). There is however no consensus as to how necessary this is or how it should be done. Since memory is a concept, not a process, many small-scale atmospheric structures could contribute to memory: Convective Kinetic Energy (Pan and Randall 1998), discharge-recharge mechanisms for the energy cycle (Yano and Plant 2012a), cold pools and their life cycle (Grandpeix and Lafore 2010; Park 2014; Del Genio et al. 2015), persistent entrainment processes (Piriou et al. 2007), or spatial organization mechanisms (Mapes and Neale 2011) are all candidates.

High-resolution simulations of moist convection are now a mainstay for process research. A simple idealized framework that has become very popular for studying simulated convection is local "Radiative-Convective Equilibrium" (RCE; Wing et al. 2017), where convection in a small domain proceeds with periodic boundaries hence no lateral sources of energy or moisture. This setting is useful to explore quasi-steady states (see Kuang 2010). Here we present an alternative and complementary idealized experiment which addresses the dynamic nature of convection. This

Accepted for publication in *Journal of the Atmospheric Sciences*. DOI10.1175/JAS-D-20-0337.1.

experiment seeks to further explore the diagnostic hypothesis and the "memory" of convection identified in previous studies, and to better understand convective instability and how it relates to convective-dynamical coupling and interaction.

This paper is organized as follows. In Section 2 we present novel numerical simulations of convection designed to isolate small-scale from large-scale behavior. In Section 3 we present a toy "predator-prey" model which emulates the dynamic behavior of convection seen in our numerical model results and in other studies published previously. In Section 4 we discuss some issues relating to our results, and we give conclusions in Section 5.

2. WRF "strong-nudging" simulations

a. Experiment design

We extend a study by Colin et al. (2019), hereafter C19, who used the WRF Cloud-Resolving Model (CRM) to numerically simulate convection in a 200-km square region over ocean at fixed surface temperature. We follow C19 in identifying the horizontal average model state as the "macrostate" ξ, and the small-scale model-resolved departures of state variables from this macrostate as the "microstate". By interrupting and restarting simulations with the same macrostate but different microstates, C19 showed that rainfall and convective activity in the model are altered for many hours, thus exhibiting "memory" of past microstates. However, in that study both the micro- and macrostates responded to the perturbations, so that their individual roles could not be isolated. Here we use the same model and setup (their unorganized-convection setup, which showed weakest memory).

However, instead of instantly changing the microstate, we hold the macrostate ξ approximately fixed to a target state. This target is the mean state obtained from an unperturbed, free run of the

Accepted for publication in *Journal of the Atmospheric Sciences*. DOI10.1175/JAS-D-20-0337.1.

same model in Radiative-Convective Equilibrium (RCE). Thus, in this experiment we simulate the evolution of convection in the mean large-scale environment in which the convection naturally occurred, but without allowing this mean environment to change or fluctuate.

In practice we implement this in WRF via a strong nudging method: we add an additional tendency term for potential temperature (T), water vapor mixing ratio (q), and horizontal winds (u, v). This term is a first-order relaxation proportional to the difference between the domain-mean value and target:

$$\frac{\partial a}{\partial t} = -\frac{\overline{a} - \overline{a}_{\text{target}}}{\tau_{\text{nudg}}} \tag{1}$$

where a is any of $\{T, q, u, v\}$ on a given model level, τ_{nudg} is the nudging time scale (40 seconds), overbars denote horizontal domain average, and $\overline{a}_{\text{target}}$ is the target value we impose. This strong nudging is maintained throughout the experiment at every grid point. The nudging terms are calculated from the difference between the horizontal mean fields and the target profiles, so that they only depend on (z, t) and are always horizontally uniform thus minimizing any effect on the microstate. Note this is not the standard WRF nudging (which nudges each grid point toward a background), and requires careful implementation due to WRF's tile architecture. This nudging does not exactly prevent deviations, it only makes them negligibly small, at least during the first phase of the simulation (see Subsection 2c).

This fixed-macrostate experiment can be thought of as an extreme form of the "weak temperature gradient" (WTG) approach (Sobel et al. 2001). In traditional WTG an implicit vertical velocity profile is applied within the column so as to nudge the free-tropospheric temperatures toward a reference profile, mimicking the effect of gravity-wave adjustment. Our procedure differs in three respects: (1) the entire column is nudged including the boundary layer, (2) the nudging is strong enough to keep the mean profile essentially pinned to the target state, and (3) the humidity (and optionally wind) fields are included in addition to temperature. This procedure, which could

Accepted for publication in *Journal of the Atmospheric Sciences*. DOI10.1175/JAS-D-20-0337.1.

also be referred to as WTHG (weak temperature and humidity gradient), is much less physically motivated than WTG—gravity waves would adjust only buoyancy (virtual temperature), not the other fields—but we present it as a conceptually simple, idealized test of convective physics (a "thought experiment").

In principle, other prognostic variables in WRF that we did not nudge (hydrometeor mixing ratios and a few others) are effectively part of the microstate and could be involved in the dynamic behavior analyzed here. However, C19 found those to be unimportant for convective memory. We therefore do not expect changes in those quantities to be important drivers of behavior and do not consider them in this study.

If the CRM domain is taken as a surrogate for a grid cell of a climate model (GCM), then the grid values in the GCM are represented by the macrostate ξ and the microstate represents the unresolved behavior whose impact must be predicted by the GCM physics. Our experiment mimics in a CRM world what would happen in a GCM by calling the physics schemes repeatedly with the same input profile of thermodynamic fields and horizontal winds (though not the same vertical velocity; see below). The nudging terms are equivalent to the standard large-scale advection terms in any GCM– the only difference being that we adjust their magnitudes so as to zero out any changes in the profile, to create a situation where the diagnostic assumption (which assumes blindness to the microstate) would lead to simple and predictable convective behaviour, enabling that assumption to be directly tested. This procedure should provide a clean distinction between the impact of the present mean environment ξ vs. the impact of past convective behavior, thus fully isolating microstate convective memory in the sense defined by C19.

Accepted for publication in *Journal of the Atmospheric Sciences*. DOI10.1175/JAS-D-20-0337.1.

b. Model settings

Our simulations follow the setup of C19, namely: we use the WRF ARW Version 3.6 (Skamarock et al. 2008) with 1 km horizontal resolution; a 6s time step; a 201x201 km doubly periodic domain; 69 levels, with the model top at 30 km and a sponge layer from 25 km upward; a uniform specified 302K water surface; no rotation; and parameterizations are the TKE turbulence (for horizontal turbulent diffusion, Skamarock et al. 2008), Yonsei University PBL (for vertical turbulent diffusion, Hong et al. 2006), MM5 surface (Jiménez et al. 2012), WSM6 microphysics (Hong and Lim 2006), and RRTMG radiation (Iacono et al. 2008). There is no diurnal cycle. The model is run for 100 days, and statistical equilibrium (RCE) is reached within 30 days. Further details on the RCE solutions in this configuration can be found in C19. Details on how strong nudging was implemented in the WRF code can be found in Colin (2020).

Nine experiment runs were conducted by restarting the original control run with strong nudging of all four variables $\{T, q, u, v\}$, beginning on one of nine selected days after day 60. For each experiment run, the nudging target profile was set to the horizontal- and time-average of the control run over the 20-day period centered on the restart day. Thus each experiment uses a slightly different target profile but all are approximately the RCE profile for this particular model and configuration.

c. Results

Under the hypothesis that convective activity can be diagnosed from the horizontal wind and thermodynamic environments alone, the convection should remain statistically steady in all experiments since these environments are steady. However, surprisingly, we instead find that within 6-11 hours, convection begins exponential growth or decay, and within a few more hours reaches either absurdly large precipitation rates $\sim$ 3000 mm day^{-1} and wind speeds $\sim$ 50-100 m s^{-1}, or else

Accepted for publication in *Journal of the Atmospheric Sciences*. DOI10.1175/JAS-D-20-0337.1.

precipitation falls to zero. Four of the nine experiments developed rapid growth of convection (one of which is shown in Fig. 1, see also supplementary figures), while five showed quasi-exponential decay to no rain (see movies provided as Supplemental Information).

Whether the result is growth or decay seems to depend on the target profile, which differs slightly among the experiments. But as the target profiles are all taken from the control (RCE) run by averaging over slightly different time periods, they differ very little; e.g., water vapor mixing ratio at 500 hPa varies by only $\sim 0.03\%$ among targets, potential temperature at the 1st model level by $\sim 0.0003\%$ (0.001 K). Thus all target profiles are almost identical. Variables derived from the target profiles also differ very little: precipitable water varies by only $\sim 0.01\%$. Further analysis reveals that one derived variable, Convective Available Potential Energy (CAPE), differs somewhat more, by up to 10 $\mathrm{J\,kg^{-1}}$ or 0.1%. Moreover these CAPE values are higher in all the growth cases than in the decay cases. This strongly suggests that CAPE and possibly other quantities decided the growth or decay outcome, despite the tiny (i.e., unobservably small) range of values. These differences are several orders of magnitude smaller than the spread of values seen in nature and so would lead to essentially identical predictions in any diagnostic convective theory. Note that CAPE is computed here by lifting the air parcel with the maximum equivalent potential temperature found in the first 3 km in a pseudo-adiabatic way and without entrainment.

At first we suspected the unstable behavior in WRF could be due to numerical or other problems, and so performed a number of tests. In particular, we tried forbidding negative water vapor mixing ratios; using multiplicative rather than additive nudging, so that the nudging of water vapor varies proportional to water vapor amount; restricting nudging to the troposphere; restricting nudging to non-cloudy points, so as not to disturb cloudy relative humidity; changing the nudging time constant; and a number of technical changes to the way the nudging was coded in WRF. These tests show that the instability is robust to how the method is implemented. But the instability

Accepted for publication in *Journal of the Atmospheric Sciences*. DOI10.1175/JAS-D-20-0337.1.

occurs only if the mean potential temperature *and* humidity profiles are both fixed; if either one is left to freely respond to changes in convection, the instability disappears. This indicates that convection can self-regulate either by increasing static stability or by dehydrating the troposphere, but if both quantities are fixed, self-regulation is prevented and the system becomes unstable. The nudging of winds has no effect on the instability. We conclude that the radiative-convective state, which is in a stable equilibrium under normal conditions, assumes an *unstable equilibrium* in a thermodynamically fixed mean environment. The nudging does not influence any microstate process but prevents the interaction between microstate and macrostate, and so "alters" part of the usual model physics: this is an "instability under forcing change" (like a Larsen effect in acoustics). This instability will be encoded into a toy model in Section 3.

Next we attempt to elucidate the instability mechanism via the external but interactive nudging terms. At the onset of exponential growth, the water vapor mixing ratio near cloud base (about 500 m) becomes slightly lower than the target, while temperature throughout the troposphere rises slightly, except at the surface where it dips very slightly (see supplementary figures). Correspondingly, the nudging tendencies work in the opposite direction, injecting dry static energy at the surface and removing it aloft, and injecting water vapor in the lower troposphere and removing it in the upper troposphere. These changes are consistent with enhanced convection and downdrafts cooling and drying the sub-cloud layer, but do not give much insight into the initial trigger of the instability.

Some hint on the internal cause of instability can be gained by carefully examining the time series of various quantities as the system enters the exponential growth phase (Fig. 2). The first variable to stray from RCE is the standard deviation of 2-m temperature (T2), followed by the standard deviation of 2-m waper vapour (Q2). Then the standard deviation of Moist Static Energy (MSE) in the sub-cloud layer and the standard deviation of CAPE start to grow, which makes sense since the

Accepted for publication in *Journal of the Atmospheric Sciences*. DOI10.1175/JAS-D-20-0337.1.

2-m temperature and humidity affect MSE and CAPE. Then the standard deviation of water vapour at 500 hPa and the vertical wind at 700 hPa start to grow. So far all of these are microstate quantities. The first macrostate quantity to change is the mean MSE in the sub-cloud layer which decreases away from its target value. Then the standard deviation of temperature at 500 hPa increases, then the mean temperature at 500 hPa increases, then the mean precipitable water decreases, then the rain rate increases. This sequence indicates the instability grows from the surface upward, starting from thermodynamic properties at the surface, then in the sub-cloud layer, then affecting winds in the lower free troposphere, then thermodynamic properties in mid-troposphere, then rain. Another important feature is that the instability starts from the microstate variables (standard deviations) and then affects the macrostate ones (means). We also examined surface fluxes and found that they only begin increasing well after the others, so they are not part of the driving mechanism.

It may seem contradictory that macrostate quantities changed at all given the experiment design, but the nudging strength is finite (Fig. 3). The difference between macrostate means and targets is extremely small at the beginning of the simulations ($\sim 10^{-4}$ K for T and $\sim 10^{-4}$ g kg^{-1} for q), and the nudging terms are correspondingly very small (e.g., $\lesssim 0.2$ K day^{-1}, much smaller than radiative cooling). But toward the end of the growth cases these differences become quite large (~ 1 K for T and $\sim 0.8\ g.kg^{-1}$ for q). By the time this happens the rainfall has reached absurd values and the convection is growing so fast that even 40-second nudging is not able to keep up, at which point we are no longer interested in the simulations. The evolution of the mean state under strong nudging is further detailed in the supplementary figures.

d. Interpretation and discussion

Our results (Fig. 2) indicate that low-level thermodynamic heterogeneities are "first movers" in the development of unstable convective growth, in agreement with previous studies (C19; Stirling

Accepted for publication in *Journal of the Atmospheric Sciences*. DOI10.1175/JAS-D-20-0337.1.

and Petch 2004; Davies et al. 2013; Daleu et al. 2020) which have reported that thermodynamic heterogeneities near the surface can strongly influence subsequent convection independently of the mean state ξ. This is consistent with longstanding meteorological studies showing the ability of cold pools, roll circulations or other features to drive or trigger convection (Weckwerth 2000; Böing et al. 2012). Such features can enhance convection either by providing more-buoyant-than-average air for updrafts (i.e., "natural selection", Tompkins (2001), Mapes and Neale (2011)), by local mechanical lifting, or by allowing updrafts to assume a larger size and thereby entrain less (e.g. Rousseau-Rizzi et al. 2017). Moreover, these near-surface thermodynamic structures are also *created* by convective downdrafts; for example cold pools are a well-recognized result of precipitation (e.g. Zuidema et al. 2017).

This implies a positive feedback. Any positive change in rain rate causes a same-signed change in downdrafts and thus boundary-layer heterogeneity associated with cold pools and other structures. These, in turn, change the updraft velocities in the same direction, reinforcing the initial change in rain rate and driving stronger vertical mixing and downdrafts. Such a positive feedback loop has already been anticipated for individual cloud systems in past studies (Böing et al. 2012). Conversely, in the non-nudged, coupled system with freely evolving ξ, a change in rain rate (hence net heating and drying) would provoke an opposite change in humidity and/or CAPE, restoring the system toward its original equilibrium. But with these macrostate quantities fixed, this stabilizing negative feedback is deactivated. We will come back to these two competing feedback mechanisms at the beginning of Section 3.

Another instability that has recently been subject to much investigation is the spontaneous transition from isolated convection to self-aggregation in numerical simulations (see Wing et al. 2017, for a review). However we think the instability found here is independent from self-aggregation. First, during the exponential growth phase convection does not show any apparent sign

Accepted for publication in *Journal of the Atmospheric Sciences*. DOI10.1175/JAS-D-20-0337.1.

of aggregation; instead the individual drafts simply strengthen and become more numerous (Fig. 1; see also supplementary movies). Second, the state can diverge from the unstable equilibrium in either direction (in half of the cases to a state of zero rain), which cannot be explained by a change in organization since the initial equilibrium is already fully disorganized. And third, self-aggregation seems to require weeks to occur, whereas our instability occurs in less than one day.

Finally we consider the role of vertical velocity. Our nudging process for the thermodynamic variables implies exogenous sources or sinks of water vapor and enthalpy, which are small at first but become large when convection drifts substantially away from its RCE state. In nature these would normally be provided mainly by ascending or descending motions within the column (i.e., low-level convergence or divergence). Thus we are, in effect, prescribing such motions calibrated so as to instantaneously negate the impacts of convection (as in WTG but for multiple fields: WTHG). Therefore, while the unstable behavior we find is inconsistent with the diagnostic assumption that convection can be diagnosed from horizontal winds, temperature, and humidity, it is not necessarily inconsistent with a diagnosis that also employs large-scale vertical velocity and horizontal advection as a predictor, since they are (implicitly) changing substantially. This question will be revisited in Section 4.

3. Predator-prey Model

The mechanisms proposed in Section 2d, whereby a positive feedback occurs between small-scale variability (e.g., boundary-layer heterogeneity) and rainfall while a negative feedback occurs through CAPE or humidity, suggest a toy model with a positive and a negative feedback loop. Physical reasoning and intuition led us to a simple predator-prey system, in which both feedback loops naturally exist (Fig. 4). Here we attempt to formulate a correspondingly simple model framed

Accepted for publication in *Journal of the Atmospheric Sciences*. DOI10.1175/JAS-D-20-0337.1.

as an ecology of structures at different scales to represent these feedbacks and to explore whether it is helpful in interpreting transient convective behavior more generally.

a. Model formulation

We characterize an isolated convective system via a variable V representing those aspects of the convective state that promote convective activity and are promoted by it, hence contributing to the positive feedback; and a state measure R representing aspects of the environment that promote convective activity but are decreased by it, hence providing a negative feedback (Fig. 5). Based on the results and discussion in Section 2d, we provisionally identify V with the microstate variability of humidity or MSE in the boundary layer, although it could also include any other aspects of the micro- or macrostate that contribute to the positive feedback on convective activity.

It is likewise not obvious what measure R of the atmospheric state best captures its susceptibility to convect, although our finding that the stability of the convective system depends on ξ being free to respond indicates that R must represent the macrostate. The two leading candidates for such a measure are CAPE and humidity, since they are each reduced by convective activity (the former by latent heat release aloft, the latter by condensation of water vapor), and each promotes convective activity, to a similar degree under realistic scalings (Mapes 2004). Thus R is taken here to represent some combination of horizontal-mean CAPE and column humidity.

These two postulated measures then interact via P, the precipitation process, in this proposed manner:

$$\frac{\partial R}{\partial t} = E_0 - P \tag{2}$$

$$\frac{\partial V}{\partial t} = -\alpha_{\text{damp}} V + \alpha_{\text{VP}} P \tag{3}$$

$$P = \alpha_P R V \tag{4}$$

Accepted for publication in *Journal of the Atmospheric Sciences*. DOI10.1175/JAS-D-20-0337.1.

Here, E_0 is the specified source of R, set to be steady at first; α_{damp} is the self-damping rate for V; α_{VP} quantifies the influence of P on V (generation of boundary-layer structure by precipitating convection), and α_P quantifies the sensitivity of P to the other variables. We also considered adding two stochastic forcing terms but for simplicity did not keep them in the default version of the model since they do not play a major role in most results presented here and are somewhat arbitrary. They do however tend to make some results better and closer to the CRM. The stochastic version of the predator-prey model and its results are described in the Supplement.

Based on our physical interpretations of R and V we can suggest a physical basis for these equations. Equation (2) is a statement of energy conservation (to the extent that R reflects CAPE) or water conservation (to the extent that R reflects the column-integrated water vapor). The model forcing E_0 can be correspondingly understood as the source of CAPE (tropospheric radiative cooling) or water vapor (surface evaporation), respectively. Both interpretations of E_0 are consistent since we consider RCE over a liquid surface, and both equate to the driving force of the hydrological cycle. Precipitation is the sink of R as it directly removes water vapor via condensation, and in so doing releases latent heat which reduces CAPE by heating the air aloft.

Equation (3) is the simplest prognostic equation for V, including a source from convection proportional to the precipitation rate, and a simple dissipative term. Note a similar equation was used by Mapes and Neale (2011) for their convective organization ("org") parameter (whose physical interpretation differed from ours for V but which plays a similar role).

Equation (4) is the simplest non-linear parameterization for P. It asserts that strong precipitation scales with both microstate variance and a favorable large-scale environment, capturing via a multiplication operation the idea familiar to forecasters that multiple "ingredients" are simultaneously necessary for convection (Doswell et al. 1996). But admittedly the exact form of this equation is

Accepted for publication in *Journal of the Atmospheric Sciences*. DOI10.1175/JAS-D-20-0337.1.

somewhat arbitrary, and for example the exponents could be other than unity. A few other possible formulations of these equations are considered in Section 4b.

If (4) is substituted into the other two equations, the result is nearly identical to the classic Lotka-Volterra "predator-prey" equations (where R is the prey and V the predator), except that here the source of new prey is constant whereas in the classic case the prey self-multiply. Note that predator-prey models have previously been proposed for shallow and aerosol-dominated convective systems (Koren and Feingold 2011; Dam et al. 2017) but not so much for deep convection. One important exception is a convective parameterization (Nober and Graf 2005) which uses a predator-prey approach to distribute convective activity among varying cloud types, but not to represent the non-linear interactions investigated here. Likewise, there is also a discrete predator-prey experiment to model the competition between cloud types (Neggers and Griewank 2021). The closest existing equations to ours are by Yano and Plant (2012a) who effectively represent convection as a variation on the predator-prey model (even though the non-linearity, motivation and interpretation are different), which creates a discharge-recharge cycle.

b. Analytical solutions

We first investigate analytical solutions to the non-stochastic version of this model. There are two steady (RCE) solutions: a trivial one with E_0, V and P all equal to zero, which is not interesting, and another with

$$R_{\mathrm{RCE}} = \frac{\alpha_{\mathrm{damp}}}{\alpha_{\mathrm{VP}}\alpha_P} \tag{5}$$

$$V_{\mathrm{RCE}} = \frac{\alpha_{\mathrm{VP}}}{\alpha_{\mathrm{damp}}} E_0 \tag{6}$$

$$P = E_0 \tag{7}$$

Accepted for publication in *Journal of the Atmospheric Sciences*. DOI10.1175/JAS-D-20-0337.1.

Interestingly, R_{RCE} is independent of the model forcing E_0, while V_{RCE} (and of course P) vary in proportion to the model forcing.

To examine time-dependent behavior near this solution, it is convenient to non-dimensionalize:

$$\begin{cases} t' & = \alpha_{\mathrm{damp}}\, t \\ R' & = \dfrac{\alpha_{\mathrm{VP}}\, \alpha_P}{\alpha_{\mathrm{damp}}}\, R \\ V' & = \dfrac{\alpha_P}{\alpha_{\mathrm{damp}}}\, V \\ P' & = \dfrac{\alpha_{\mathrm{VP}}\, \alpha_P}{{\alpha_{\mathrm{damp}}}^2}\, P \\ {E_0}' & = \dfrac{\alpha_{\mathrm{VP}}\, \alpha_P}{{\alpha_{\mathrm{damp}}}^2}\, E_0. \end{cases} \tag{8}$$

Combining P', we have the canonical system:

$$\begin{cases} \dfrac{\partial R'}{\partial t'} & = {E_0}' - R'\, V' \\ \dfrac{\partial V'}{\partial t'} & = V'\, (R' - 1) \\ P' & = R'\, V' \end{cases} \tag{9}$$

Then the stationary solution becomes $R'_{\mathrm{RCE}} = 1$ and $V'_{\mathrm{RCE}} = E'_0$, and we can consider nearby solutions by substituting $R' = 1 + x$, $V' = E'_0 + y$.

The full equation system for the departures (x, y) from the stationary solution becomes:

$$\begin{cases} \dfrac{\partial x}{\partial t'} & = -y - ({E_0}' + y)\, x \\ \dfrac{\partial y}{\partial t'} & = ({E_0}' + y)\, x \end{cases} \tag{10}$$

Linearizing about the solution $x = y = 0$, differentiating the first equation with respect to t', and substituting this into the second yields

$$\frac{\partial^2 x}{\partial {t'}^2} + {E_0}' \frac{\partial x}{\partial t'} + {E_0}' x = 0, \tag{11}$$

Accepted for publication in *Journal of the Atmospheric Sciences*. DOI10.1175/JAS-D-20-0337.1.

the equation of the damped harmonic oscillator. Accordingly we predict damped oscillations of angular frequency $\sqrt{E_0{}'}$ in nondimensional time units, or

$$\sqrt{\alpha_{\mathrm{VP}}\alpha_P E_0}$$

in dimensional units. A fully nonlinear analytical solution of the equations does not appear tractable; for example the separation-of-variables approach of Yano and Plant (2012a) for a similar model does not work in our case. We instead numerically time-integrate the full predator-prey model using simple forward differencing.

c. Fixed-macrostate behavior of the predator-prey model

Imposing the macrostate in the predator-prey model, as in the strong nudging WRF experiments presented in Section 2, means fixing R to a constant R_0 such that $R_0 = R_{\mathrm{RCE}}(1+\varepsilon) \approx R_{\mathrm{RCE}}$. Fixing R this way, equation (2) is removed and the model reduces to a single equation

$$\frac{\partial V}{\partial t} = \alpha_{\mathrm{VP}}\,\alpha_P\,(R_0 - R_{\mathrm{RCE}})\,V \tag{12}$$

with an exponential solution in time whose growth rate is proportional to $R_0 - R_{\mathrm{RCE}}$. Thus the model predicts the existence of an unstable equilibrium at the RCE state, as implied in the WRF simulations with strong nudging (Section 2). If R_0 is less than R_{RCE} by however little—as in half of the WRF simulations—P will eventually go to zero. If R_0 is greater, P will diverge to infinity (or, in WRF, to an extreme value that the predator-prey model does not try to predict).

Numerical integrations of the predator-prey model with fixed macrostate and no stochastic terms confirm that, in agreement with the analytical solution, it produces the same exponential growth or decay as the CRM simulations under fixed-macrostate conditions (Fig 6). This is not really a strong test of the model since it was chosen to capture this instability, so we will now present a different test to check its validity.

Accepted for publication in *Journal of the Atmospheric Sciences*. DOI10.1175/JAS-D-20-0337.1.

d. Tests of response to change in microstate

We now use the predator-prey model to perform simulation ensembles equivalent to the 3D convection-permitting experiments of C19. In that study, selected microstate variables were homogenized (reset) to horizontally uniform values and the run restarted, with an average trajectory computed over multiple realizations. In particular, homogenizing low-level humidity and temperature caused precipitation to crash to a low value, then overshoot the equilibrium value briefly, then recover to the equilibrium value as for a slow, damped oscillation. The equivalent experiment in the predator-prey model is to reset V to zero at an arbitrary time and then continue integration. Ensembles of 100-1000 members are used.

To make this comparison also requires specifying definitions of R and V in order to estimate relevant values from WRF. Our preliminary choices are respectively the mean and standard deviation of the sub-cloud layer water vapor mixing ratio (below 600 m). The near-surface specific humidity simultaneously contributes to CAPE and to column-integrated water vapor, making it an advantageous choice for R, and the variation of this quantity was the single strongest "memory" variable found in C19 (see Section 2d). We must also set values for the three α parameters in the predator-prey model; the default parameters $\alpha_{\text{damp}} = 0.3$, $\alpha_{\text{VP}} = 0.5$, and $\alpha_P = 0.1$ (in arbitrary units for simplicity) were chosen to optimise the comparison between the predator-prey model and C19 (noting that, as shown above, the “ringing frequency” of the linearized system is determined by the product of the last two of these).

The behavior with these parameters is qualitatively close to that of the C19 WRF results (Fig. 7), with one time unit in the predator-prey model equating to 12.4 minutes in WRF if we choose the unorganised WRF simulation of C19 as a reference. The other C19 organisation types lead to qualitatively similar behaviour but with a slower recovery (see Supplement, see C19’s Fig. 7 and

Accepted for publication in *Journal of the Atmospheric Sciences*. DOI10.1175/JAS-D-20-0337.1.

9). The WRF runs are only 24 hours long which does not allow to use the WRF organised cases to fully compare with the behaviour of the predator-prey model, so we keep the WRF unorganised case as a reference. Since time in the predator-prey model is arbitrary, the chosen time scaling is a subjective choice to optimize visual comparison between WRF and predator-prey oscillations. With other definitions of R (CAPE or precipitable water), shown in Fig. 8, the agreement is less good but still not bad. We did not attempt to optimize R from these experiments, but definitions could potentially be found combining multiple convective variables that would further improve agreement between the two models.

We now analyze the sensitivity of this result to α_{damp}, the V damping rate (Fig. 9). One could hypothesize that the more damped V is, the faster memory is lost in the system. With a larger damping coefficient, the oscillations have a smaller amplitude, which is consistent with this intuition. Nevertheless, the oscillation frequency changes only slightly with large changes in damping coefficient, showing that the oscillation time is not affected by this parameter. This result is consistent with our linearized solution (Eq. (11)), whose frequency did not depend on this parameter, supporting the ability of this solution to capture the key aspects of the model. We also confirm (Supplement) that the stochastic forcing terms do not affect the results much, which is reassuring. We also tested the sensitivity of results to variations in the α parameters; as expected they affect the oscillation period, but the general character of the response is not very sensitive to them (see Colin 2020, for further details).

We note that the microstate 'reset' (homogenization) employed by C19 was rather brutal in completely eliminating the structure in one variable while leaving others untouched; resetting all variables to a "quiet" variability level characteristic of undisturbed conditions would have been more representative. However C19 reported that for disorganized convection, as long as some

Accepted for publication in *Journal of the Atmospheric Sciences*. DOI10.1175/JAS-D-20-0337.1.

variables are unhomogenized, some structure relatively quickly re-forms in the others, suggesting the results of the experiments considered here may not be qualitatively affected by this choice.

e. Predicted responses to external periodic model forcing

During the passage of a larger-scale wave ascent will act as a source of R, and descent as a sink, whereas such waves would not be expected to significantly affect V. Thus we can test the model's prediction of the convective response to waves by imposing a periodic source of R, which following equation (2) is achieved via modulation of E_0. This is done by setting one time unit in the predator-prey model to 69 min in WRF, which is the appropriate time scaling for the wind-shear-organised case in Colin et al. (2019), arguably the most realistic case (for comparison this time scale was 12.4 min for the disorganized case and over two hours for the self-aggregated case). So the scaling chosen here is near the middle of this spread.

The result depends on the period of model forcing E_0. At long periods ($\gg$ 1 week), all three model variables vary in phase (Fig. 10a). At short periods less than one day (Fig. 10c), V varies little and P and R lag the forcing by 90°. But when forced near the 3-day time scale typical of tropical wave disturbances (Reed and Recker 1971), the precipitation varies almost exactly with the forcing, due to R leading the forcing and V lagging it (Fig. 10b). This behavior is very interesting, because it matches the observation (used to support "quasi-equilibrium" assumptions for convection) that convective heating closely follows the forcing, on time scales approaching the diurnal time scale (Arakawa and Schubert 1974). Although there is no direct dependency of P on E_0 in this model, the results are consistent with a precipitation response time scale τ_P such that P is in phase with the forcing when forced slower than τ_P, but P lags when forced on faster time scales than τ_P.

One of the noted difficulties of current atmospheric models is the representation of the diurnal cycle of convection over land, with most traditional models simulating onset close to noon (when

Accepted for publication in *Journal of the Atmospheric Sciences*. DOI10.1175/JAS-D-20-0337.1.

CAPE peaks) whereas in observations it typically occurs late in the afternoon (Couvreux et al. 2015). The diurnal cycle on land is driven by the heating of the surface by the sun during daytime. This forcing can be represented very crudely in our model by imposing a square-wave modulation of the model forcing E_0. On this time scale the physical interpretation of R becomes important since daytime solar heating is a source of CAPE, but can provide water vapor only via surface evaporation; thus we suppose here that R variations reflect those of CAPE to some significant extent.

When forced in this way the model correctly shows R (CAPE) peaking near midday but rainfall P peaking later in the afternoon (Fig. 10d). For this particular aspect, this is a strength compared to many GCMs, although some GCMs have succeeded in finding ways to delay the diurnal cycle (e.g. Rio et al. 2009; Bechtold et al. 2014). The delay of precipitation in the predator-prey model is because of the time required to build up V which is also needed for precipitation and does not peak until the evening. The afternoon peak in precipitation occurs when there is still substantial CAPE but microstate variability has also built up. This result depends on the time scale assigned to the predator-prey model, meant to be equivalent to the CRM response time scale to homogenization, which is sensitive to the level of convective organisation in the CRM (see C19). For example, using the very short response time for unorganised convection leads to a midday maximum of P. Thus the result only demonstrates plausibility that convective memory as represented in the predator-prey model could account for the delayed diurnal cycle over land, in which case a strong role for organisation is also implied.

f. Observed lag relationships

The lag relationships inherent in the predator-prey model are readily visible in observations composited according to rain rate (Fig. 11). The rainfall data are from the Manus ARM Present

Accepted for publication in *Journal of the Atmospheric Sciences*. DOI10.1175/JAS-D-20-0337.1.

Weather Detector (similar results are obtained from the other available gauges). Data were composited around heavy-precipitation events, which are defined when the 1-minute precipitation is in the highest 0.5% of all precipitation values (i.e., greater than 15 mm/hr; results not qualitatively sensitive to this threshold). The mean and standard deviation at each lag δt are computed from the corresponding statistics of all observation pairs, where each pair consists of one environment observation at time $t - \delta t$ and one (high) precipitation observation at time t. Interpreting variability between elements of the composite ensemble as spatial standard deviation requires an ergodic assumption that the distribution across an ensemble is equivalent to the small-scale distribution within a single member. Results show that mean near-surface temperature and humidity (which govern CAPE) rise slightly heading into the storm, then decrease rapidly when precipitation picks up (like R); thermodynamic variability near the surface begins building when precipitation is still low, then grows throughout the period of high precipitation, decaying slowly afterward (like V). Previously published composites based on radiosonde data (Sherwood and Wahrlich 1999) confirm that the evolution of CAPE around precipitation peaks qualitatively reflects that shown here for near-surface temperature and humidity.

4. Discussion

a. On the predator-prey model equations

The model presented here is extremely simple in characterizing the atmospheric macrostate by a single variable R. We have argued that for the qualitative behavior explored here one could identify R successfully with either CAPE or some measure of humidity. In reality convection will be regulated by multiple features of the water-vapor and temperature profiles, and by wind

Accepted for publication in *Journal of the Atmospheric Sciences*. DOI10.1175/JAS-D-20-0337.1.

shear. To further extend this idea might require developing at least a three-variable model in which instability and humidity are treated separately, but we leave this as a future goal.

As for V, while a consistent story emerges wherein V represents near-surface heterogeneity (Section 2d), we cannot rule out other contributors to V and hence convective inertia or memory. In principle V could represent any durable feature of the atmospheric macro- or microstate that promotes, and is promoted by, convection. In particular, previous studies have proposed shallow convection plays an important role as a transitional state (Rio et al. 2009; Waite and Khouider 2010; Yano and Plant 2012b, 2020) which moistens the mid-troposphere hence enabling convective deepening, explaining the delay in convective growth. Previous composite studies (Sherwood and Wahrlich 1999, their Fig.5) do show mean moisture from 800-400 hPa following a trajectory roughly similar to that shown here for near-surface moisture variability (Fig. 11b), at least around precipitation peaks. Though mid-level moisture is clearly an important regulator of convection, however, it might be controlled more by large-scale forcings than by previous convection. For example, Hohenegger and Stevens (2013) concluded that mid-level moistening by shallow convection is too weak to account for rapid deepening of convection. Also, interpreting V as near-surface heterogeneity rather than mean mid-tropospheric humidity seems more consistent with the role of the microstate in the instability seen in the WRF strong-nudging simulations (Section 2).

It is interesting to compare the assumptions of our model—in particular equation (4)—with those seen in typical convective schemes. Such schemes normally have a "trigger" condition required for convection to activate, thus introducing a non-linear element. In some schemes (Gregory and Rowntree 1990; Emanuel 1991) the presence of CAPE or buoyancy in the lower troposphere is sufficient to trigger convection, and these or similar quantities also regulate the intensity of convection once triggered (since this control variable cannot increase too much without generating convection, such schemes come closest to "quasi-equilibrium" behavior). Other schemes trigger on

Accepted for publication in *Journal of the Atmospheric Sciences*. DOI10.1175/JAS-D-20-0337.1.

a condition which does not involve CAPE, such as low-level lifting or weak convective inhibition; CAPE can then increase with no limits as long as this other condition is not met. Our non-linear predator-prey model effectively replaces these binary "triggers" with a continuous regulator in the form of V, which depends on past convection rather than any other feature of the sounding such as CIN. As such, the model would require some modification to work in non-precipitating situations, although it could potentially be useful in representing the transition from drizzling to strong convection or vice versa.

b. Other possible versions of the predator-prey model

(i) Diagnostic version. An obvious simplification is to eliminate equation (3) and set V to unity, eliminating the prognostic memory variable. In this "diagnostic" version we obtain solutions of exponential decay toward a stable equilibrium at $R_{\mathrm{RCE}} = E_0/\alpha_P$. However, we cannot carry out the microstate-reset test in Section 3d because there is no microstate variable: the model cannot capture the perturbation so predicts no response. In this version, we can still represent the strong-nudging experiment by setting $R = R_0 = R_{\mathrm{RCE}}(1 + \varepsilon)$ in place of (2) (where $\varepsilon \ll 1$ is a small number representing misalignment between the target state and true equilibrium of the full system); this yields a steady solution near the true equilibrium of the full system (all variables are then diagnostic), in contrast to the instability seen in WRF. A diagnostic version of the predator-prey model thus does not capture either WRF experiment discussed here.

(ii) Moisture-Convergence version I. Equation (4) assumes that precipitation responds only to the thermodynamic state (R) and the microstate variability, not directly to forcing (i.e., grid-scale ascent rate, moisture convergence, or rate of increase of CAPE) as it often does to some extent in convective schemes. We could emulate a "moisture convergence" approach in which rain is

Accepted for publication in *Journal of the Atmospheric Sciences*. DOI10.1175/JAS-D-20-0337.1.

directly tied to model forcing by replacing (4) by $P = E_0$, but this would yield a model in which R is constant. This model is too simple; something other than the forcing must influence convection.

(iii) Moisture-Convergence version II. We could put R-dependence back in via $P = \alpha_P R E_0$. With fixed E_0, we get the same basic behavior as with the "diagnostic" version (i) (for R and P, though not for V), so again the model does not agree with either WRF experiment. With oscillating E_0 (about a non-zero mean), R converges to its RCE value. Once it reaches this value, precipitation ends up in phase with E_0 on all time scales. Thus this model might represent slow behavior, but would fail on the diurnal cycle for example.

(iv) Moisture-Convergence version III. Restoring R, V, and forcing dependence via

$$P = \alpha_P R V E_0 \tag{13}$$

yields the same solutions as the original model when E_0 is fixed, assuming α_P is suitably rescaled. However the solutions are quite different for time-varying E_0 (see Fig. 12): for slow model forcing, R shows the opposite relation to P from what is expected or seen in the original version, and the diurnal cycle of P is shifted slightly earlier in the day rather than later as observed.

Thus, while we have surely not exhausted all possibilities, the only simple representation we are able to find that performs well in the various tests is one in which a memory variable V is represented, and in which the precipitation depends on this and on R, but not directly on the "forcing" E_0. Most current convective schemes, however, do rely on vertical velocity or other quantities closely related to such forcing (Doswell et al. 1996; Banacos and Schultz 2005; Peters et al. 2013; Suhas and Zhang 2014, 2015). We speculate that the reason this has proven helpful is because (as our strong-nudging experiments show) it is not possible to diagnose convective rainfall successfully from ξ alone, and using the forcing may help with this even though in our particular model it is not as good as explicitly keeping track of a memory variable V.

Accepted for publication in *Journal of the Atmospheric Sciences*. DOI10.1175/JAS-D-20-0337.1.

c. Caveats and limitations of the study

This study uses highly idealized CRM experiments. At 1-km grid spacing, all convective scales cannot be fully resolved. And the domain size is relatively small, so that the RCE fluctuations are still noticeable. The CRM tests employed here (fixed-macrostate, microstate homogenization) involve strong perturbations and unrealistic situations. While we believe they reveal fundamental aspects of convection, it is also possible that a reasonable working model of convection could perform badly in these tests yet still do a good job in realistic situations. However, the fact that a very simple predator-prey model *does* seem to pass the tests presented here suggests that it should be possible to devise convective theories and parameterizations that can do so. Although we have proposed our best interpretation of the CRM results, one may wish to put forward other valid explanations.

The predator-prey model was only tested for three specific idealized experiments, but one may wish to impose other tests. Our predator-prey model forcing E_0 is not exactly the same as large-scale forcing, so interpreting the forcing is limited. This model is a dynamical system model: despite its limited scope, several studies have recognized some benefit in this approach (Yano and Plant 2012a; Wolding et al. 2020; Yano et al. 2020). The predator-prey model of convection is somehow based on a mean and variance description, which is a limited point of view which disregards the complexity of small-scale spatial structures: since other moments of the PDF and/or spatial coherence are missing in our model, we cannot expect too much from it. It is therefore mostly a proof of concept.

5. Conclusion

We conducted novel Cloud-Resolving Model (CRM) simulations in an enclosed domain, which show that if the domain-average temperature and humidity profiles are fixed, no stable equilibrium

Accepted for publication in *Journal of the Atmospheric Sciences*. DOI10.1175/JAS-D-20-0337.1.

exists. This is true even if the profiles are fixed as close as possible to the model's self-generated Radiative-Convective Equilibrium (RCE) profile. We find that convection eventually either grows or decays exponentially to a state vastly different from RCE. The choice between growth and decay is mediated by immeasurably small differences in CAPE (of order 10 J/kg) between the imposed profile and the unstable RCE profile. This shows that convection remains stable only if allowed to interact with at least the mean temperature or humidity field. We interpret this result in terms of a positive feedback that works through small-scale structures in the convective system, and a negative feedback that works through the thermodynamic mean state. When the mean state is held fixed, the negative feedback is deactivated so the system becomes unstable.

To formalize this we then presented a two-variable "predator-prey" model in which small-scale, near-surface structure V (the predator) promotes, and is promoted by convective precipitation P, while large-scale environmental conditions (CAPE and/or humidity, R, the prey) promote but are depleted by convective precipitation. Both variables V and R obey very simple conservation equations, while P is diagnosed from them. The buildup of V takes time, causing responses of convective rainfall P to lag changes in the environment R. This model encapsulates the feedback loops inferred from the CRM experiments and behaves consistently with them (exponential growth or decay when the mean state is fixed). Additionally it qualitatively reproduces the results of previously published CRM experiments where RCE is perturbed by eliminating small-scale variability ("homogenization"). It also captures lag relationships found in observations at tropical sites. Finally, it can reproduce the observed delay of precipitation in the diurnal cycle, although this ability relies on a time scaling that is sensitive to the degree of organisation assumed for convection.

When harmonic forcing is imposed, representing a passing wave disturbance, the response depends on the forcing period. Slowly varying forcing causes all variables to vary in near equilibrium with the forcing. Given a reasonable model time scaling, forcing on a few-day (synoptic) time scale

Accepted for publication in *Journal of the Atmospheric Sciences*. DOI10.1175/JAS-D-20-0337.1.

is too fast for all quantities to remain in equilibrium, but since both the precipitation and the forcing E_0 lag R by a similar degree, the precipitation remains roughly in phase with forcing E_0. Thus the model can predict the observed close correlation between these two quantities even on relatively short time scales, which motivates the concept of "convective quasi-equilibrium", even though the two quantities are not directly linked in the model. When forcing speeds up to sub-diurnal, the precipitation lags the forcing as expected (for example in the case of forced diurnal cycles). Thus the model seems to be qualitatively successful across a wide range of time scales (though probably not scales shorter than a few hours). Experimenting with other forms of the predator-prey model suggests that representations in which precipitation responds directly to the forcing, or in which no memory variable is included, are not as good: they are at best successful in only some of the tests presented here, if any. This line of reasoning will be investigated further in future work, where we will directly test convective schemes in current use.

The CRM tests presented here are extremely idealized, and the predator-prey model extremely simple. Nonetheless, these results may have implications for the study of convection and for its representation in models. First, our CRM results demonstrate that the environmental thermodynamic and wind profile of the large scale is fundamentally insufficient by itself to adequately determine the simultaneous convective behavior, even though the two may exhibit correlations. This is relevant for convective parameterization since it challenges the diagnostic assumption. But it also means that, for example, quantification of small-scale variability should be a priority alongside the large-scale variables traditionally targeted in convection-relevant field programs. Second, our predator-prey results suggest that it may be possible to reproduce observed relationships between forcing (i.e., moisture convergence or CAPE generation) and convective precipitation as emergent properties, without building them into parameterizations. Models of convection would likely benefit from including some prognostic measure of microscale heterogeneity (microstate memory).

Accepted for publication in *Journal of the Atmospheric Sciences*. DOI10.1175/JAS-D-20-0337.1.

Although some current convective schemes do incorporate memory of past convective states, it is unclear whether any of these do so intensively enough to reproduce the instability found here. This could be a crucial test of such schemes.

Acknowledgments. We acknowledge Claire Carouge, the ARC Centre of Excellence for Climate Extremes, and David Fuchs for assistance with WRF, and Vishal Dixit, George Craig, Robert Plant, Sandrine Bony, Takeshi Izumo, Tim Duty, and Jason Evans for useful discussions. We thank Jun-Ichi Yano and two anonymous reviewers for thoughtful reviews and critical discussion which strongly helped improve the content and style of the paper. We acknowledge NCI Australia (National Computational Infrastructure) for providing computational time. Observational data were obtained from the Atmospheric Radiation Measurement (ARM) User Facility, a US Department of Energy Office of Science user facility managed by the Office of Biological and Environmental Research. The WRF model is provided by NCAR. SCS was funded by ARC FL150100035; M. Colin was supported by CE110001028.

Data availability statement. Essential scripts and data can be accessed from a Zenodo repository created via GitHub with the DOI: 10.5281/zenodo.4243093 (Colin and Sherwood 2020). It contains scripts (in Python and NCL mostly) that were used to create and analyse the data for the paper, and some small netcdf data files created during post-processing of the original data. Original data, secondary data, and other scripts used in the analysis are archived on the Australian National Computational Infrastructure and the University of New South Wales computers: they can be obtained upon request. The ARM data can be obtained from the ARM user facility.

Accepted for publication in *Journal of the Atmospheric Sciences*. DOI10.1175/JAS-D-20-0337.1.

References

Arakawa, A., 2004: The cumulus parameterization problem: Past, present, and future. *Journal of Climate*, **17 (13)**, 2493–2525, URL http://dx.doi.org/10.1175/1520-0442(2004)017<2493:RATCPP>2.0.CO;2.

Arakawa, A., and W. H. Schubert, 1974: Interaction of a cumulus cloud ensemble with the large-scale environment, Part I. *Journal of the Atmospheric Sciences*, **31 (3)**, 674–701, URL http://dx.doi.org/10.1175/1520-0469(1974)031<0674:IOACCE>2.0.CO;2.

Bador, M., M. G. Donat, O. Geoffroy, and L. V. Alexander, 2018: Assessing the robustness of future extreme precipitation intensification in the CMIP5 ensemble. *Journal of Climate*, **31 (16)**, 6505–6525, URL https://doi.org/10.1175/JCLI-D-17-0683.1.

Banacos, P. C., and D. M. Schultz, 2005: The use of moisture flux convergence in forecasting convective initiation: Historical and operational perspectives. *Weather and Forecasting*, **20 (3)**, 351–366, URL https://doi.org/10.1175/WAF858.1.

Bechtold, P., N. Semane, P. Lopez, J.-P. Chaboureau, A. Beljaars, and N. Bormann, 2014: Representing equilibrium and nonequilibrium convection in large-scale models. *Journal of the Atmospheric Sciences*, **71 (2)**, 734–753, URL https://doi.org/10.1175/JAS-D-13-0163.1.

Böing, S. J., H. J. J. Jonker, A. P. Siebesma, and W. W. Grabowski, 2012: Influence of the subcloud layer on the development of a deep convective ensemble. *Journal of the Atmospheric Sciences*, **69 (9)**, 2682–2698, URL https://doi.org/10.1175/JAS-D-11-0317.1.

Bougeault, P., and J. F. Geleyn, 1989: Some problems of closure assumption and scale dependency in the parameterization of moist deep convection for numerical weather prediction. *Meteorology and Atmospheric Physics*, **40 (1)**, 123–135, URL https://doi.org/10.1007/BF01027471.

Accepted for publication in *Journal of the Atmospheric Sciences*. DOI10.1175/JAS-D-20-0337.1.

Castelvecchi, D., 2017: On the trail of turbulence. *Nature*, **548**, 382–383.

Colin, M., 2020: Convective memory, and the role of cold pools. Ph.D. thesis, UNSW Sydney, Sydney, Australia, URL http://handle.unsw.edu.au/1959.4/70757, 356 pp.

Colin, M., and S. Sherwood, 2020: Data for the the paper: Atmospheric convection as an unstable predator-prey process with memory. Zenodo, URL https://doi.org/10.5281/zenodo.4243093, Funding by the Australian Research Council CE110001028, doi:10.5281/zenodo.4243093.

Colin, M., S. Sherwood, O. Geoffroy, S. Bony, and D. Fuchs, 2019: Identifying the sources of convective memory in cloud-resolving simulations. *Journal of the Atmospheric Sciences*, **76 (3)**, 947–962, URL https://doi.org/10.1175/JAS-D-18-0036.1.

Couvreux, F., and Coauthors, 2015: Representation of daytime moist convection over the semi-arid tropics by parametrizations used in climate and meteorological models. *Quarterly Journal of the Royal Meteorological Society*, **141 (691)**, 2220–2236, URL https://rmets.onlinelibrary.wiley.com/doi/abs/10.1002/qj.2517.

Daleu, C. L., R. S. Plant, S. J. Woolnough, A. J. Stirling, and N. J. Harvey, 2020: Memory properties in cloud-resolving simulations of the diurnal cycle of deep convection. *Journal of Advances in Modeling Earth Systems*, **12 (8)**, URL https://agupubs.onlinelibrary.wiley.com/doi/abs/10.1029/2019MS001897.

Dam, M., M. Brøns, J. Juul Rasmussen, V. Naulin, and J. S. Hesthaven, 2017: Sparse identification of a predator-prey system from simulation data of a convection model. *Physics of Plasmas*, **24 (2)**, 022 310, URL https://doi.org/10.1063/1.4977057.

Accepted for publication in *Journal of the Atmospheric Sciences*. DOI10.1175/JAS-D-20-0337.1.

Davies, L., R. S. Plant, and S. H. Derbyshire, 2009: A simple model of convection with memory. *Journal of Geophysical Research: Atmospheres*, **114 (D17)**, URL http://dx.doi.org/10.1029/2008JD011653.

Davies, L., R. S. Plant, and S. H. Derbyshire, 2013: Departures from convective equilibrium with a rapidly varying surface forcing. *Quarterly Journal of the Royal Meteorological Society*, **139 (676)**, 1731–1746, URL http://dx.doi.org/10.1002/qj.2065.

Del Genio, A. D., 2012: Representing the sensitivity of convective cloud systems to tropospheric humidity in general circulation models. *Surveys in Geophysics*, **33 (3)**, 637–656, URL https://doi.org/10.1007/s10712-011-9148-9.

Del Genio, A. D., J. Wu, A. B. Wolf, Y. Chen, M.-S. Yao, and D. Kim, 2015: Constraints on cumulus parameterization from simulations of observed MJO events. *Journal of Climate*, **28 (16)**, 6419–6442, URL http://dx.doi.org/10.1175/JCLI-D-14-00832.1.

Doswell, C. A., H. E. Brooks, and R. A. Maddox, 1996: Flash flood forecasting: An ingredients-based methodology. *Weather and Forecasting*, **11 (4)**, 560–581, URL https://doi.org/10.1175/1520-0434(1996)011<0560:FFFAIB>2.0.CO;2.

Emanuel, K. A., 1991: A scheme for representing cumulus convection in large-scale models. *Journal of the Atmospheric Sciences*, **48 (21)**, 2313–2335, URL http://dx.doi.org/10.1175/1520-0469(1991)048<2313:ASFRCC>2.0.CO;2.

Emanuel, K. A., J. David Neelin, and C. S. Bretherton, 1994: On large-scale circulations in convecting atmospheres. *Quarterly Journal of the Royal Meteorological Society*, **120 (519)**, 1111–1143, URL http://dx.doi.org/10.1002/qj.49712051902.

Accepted for publication in *Journal of the Atmospheric Sciences*. DOI10.1175/JAS-D-20-0337.1.

Gottwald, G. A., K. Peters, and L. Davies, 2016: A data-driven method for the stochastic parametrisation of subgrid-scale tropical convective area fraction. *Quarterly Journal of the Royal Meteorological Society*, **142 (694)**, 349–359, URL https://rmets.onlinelibrary.wiley.com/doi/abs/10.1002/qj.2655.

Grandpeix, J.-Y., and J.-P. Lafore, 2010: A density current parameterization coupled with Emanuel's convection scheme. Part I: The models. *Journal of the Atmospheric Sciences*, **67 (4)**, 881–897, URL http://dx.doi.org/10.1175/2009JAS3044.1.

Gregory, D., and P. R. Rowntree, 1990: A mass flux convection scheme with representation of cloud ensemble characteristics and stability-dependent closure. *Monthly Weather Review*, **118 (7)**, 1483–1506, URL https://doi.org/10.1175/1520-0493(1990)118<1483:AMFCSW>2.0.CO;2.

Hohenegger, C., and B. Stevens, 2013: Preconditioning Deep Convection with Cumulus Congestus. *Journal of the Atmospheric Sciences*, **70 (2)**, 448–464, URL https://doi.org/10.1175/JAS-D-12-089.1.

Hong, S.-Y., and J.-O. J. Lim, 2006: The WRF single-moment 6-class microphysics scheme (WSM6). *Journal of the Korean Meteorological Society*, **42 (2)**, 129–151.

Hong, S.-Y., Y. Noh, and J. Dudhia, 2006: A new vertical diffusion package with an explicit treatment of entrainment processes. *Monthly Weather Review*, **134 (9)**, 2318 – 2341, doi:10.1175/MWR3199.1, URL https://journals.ametsoc.org/view/journals/mwre/134/9/mwr3199.1.xml.

Hwong, Y. L., and Coauthors, 2021: Characterizing convection schemes using their responses to imposed tendency perturbations. *Journal of Advances in Modeling Earth Systems*, **13 (5)**, doi:https://doi.org/10.1029/2021MS002461.

Accepted for publication in *Journal of the Atmospheric Sciences*. DOI10.1175/JAS-D-20-0337.1.

Iacono, M. J., J. S. Delamere, E. J. Mlawer, M. W. Shephard, S. A. Clough, and W. D. Collins, 2008: Radiative forcing by long-lived greenhouse gases: Calculations with the AER radiative transfer models. *Journal of Geophysical Research: Atmospheres*, **113 (D13)**, URL https://agupubs.onlinelibrary.wiley.com/doi/abs/10.1029/2008JD009944.

Jiang, X., and Coauthors, 2015: Vertical structure and physical processes of the Madden-Julian oscillation: Exploring key model physics in climate simulations. *Journal of Geophysical Research: Atmospheres*, **120 (10)**, 4718–4748, URL http://dx.doi.org/10.1002/2014JD022375, 2014JD022375.

Jiménez, P. A., J. Dudhia, J. F. González-Rouco, J. Navarro, J. P. Montávez, and E. García-Bustamante, 2012: A revised scheme for the WRF surface layer formulation. *Monthly Weather Review*, **140 (3)**, 898–918, doi:10.1175/MWR-D-11-00056.1.

Jirak, I. L., and W. R. Cotton, 2007: Observational analysis of the predictability of mesoscale convective systems. *Weather and Forecasting*, **22 (4)**, 813–838, URL https://doi.org/10.1175/WAF1012.1.

Jones, T. R., and D. A. Randall, 2011: Quantifying the limits of convective parameterizations. *Journal of Geophysical Research: Atmospheres*, **116 (D8)**, URL http://dx.doi.org/10.1029/2010JD014913.

Koren, I., and G. Feingold, 2011: Aerosol–cloud–precipitation system as a predator-prey problem. *Proceedings of the National Academy of Sciences*, **108 (30)**, 12 227–12 232, doi:10.1073/pnas.1101777108, URL http://www.pnas.org/content/108/30/12227.

Kuang, Z., 2010: Linear response functions of a cumulus ensemble to temperature and moisture perturbations and implications for the dynamics of convectively coupled waves. *Journal of the*

Accepted for publication in *Journal of the Atmospheric Sciences*. DOI10.1175/JAS-D-20-0337.1.

Atmospheric Sciences, **67 (4)**, 941–962, URL https://doi.org/10.1175/2009JAS3260.1.

Madonna, E., D. Ginsbourger, and O. Martius, 2018: A Poisson regression approach to model monthly hail occurrence in Northern Switzerland using large-scale environmental variables. *Atmospheric Research*, **203**, 261 – 274, doi:https://doi.org/10.1016/j.atmosres.2017.11.024.

Mapes, B., and R. Neale, 2011: Parameterizing convective organization to escape the entrainment dilemma. *Journal of Advances in Modeling Earth Systems*, **3**, 20 pp., doi: 10.1029/2011MS000042, art. M06004.

Mapes, B. E., 2004: Sensitivities of cumulus-ensemble rainfall in a cloud-resolving model with parameterized large-scale dynamics. *Journal of the Atmospheric Sciences*, **61 (18)**, 2308–2317, URL https://doi.org/10.1175/1520-0469(2004)061<2308:SOCRIA>2.0.CO;2.

Neggers, R. A. J., and P. J. Griewank, 2021: A binomial stochastic framework for efficiently modeling discrete statistics of convective populations. *Journal of Advances in Modeling Earth Systems*, **13 (3)**, doi:https://doi.org/10.1029/2020MS002229.

Nober, F. J., and H. F. Graf, 2005: A new convective cloud field model based on principles of self-organisation. *Atmospheric Chemistry and Physics*, **5 (10)**, 2749–2759, doi:10.5194/acp-5-2749-2005, URL https://www.atmos-chem-phys.net/5/2749/2005/.

Pan, D.-M., and D. D. A. Randall, 1998: A cumulus parameterization with a prognostic closure. *Quarterly Journal of the Royal Meteorological Society*, **124 (547)**, 949–981, URL http://dx.doi.org/10.1002/qj.49712454714.

Park, S., 2014: A unified convection scheme (UNICON). Part I: Formulation. *Journal of the Atmospheric Sciences*, **71 (11)**, 3902–3930, URL http://dx.doi.org/10.1175/JAS-D-13-0233.1.

Accepted for publication in *Journal of the Atmospheric Sciences*. DOI10.1175/JAS-D-20-0337.1.

Peters, K., C. Jakob, L. Davies, B. Khouider, and A. J. Majda, 2013: Stochastic behavior of tropical convection in observations and a multicloud model. *Journal of the Atmospheric Sciences*, **70 (11)**, 3556–3575, URL http://dx.doi.org/10.1175/JAS-D-13-031.1.

Piriou, J.-M., J.-L. Redelsperger, J.-F. Geleyn, J.-P. Lafore, and F. Guichard, 2007: An approach for convective parameterization with memory: Separating microphysics and transport in grid-scale equations. *Journal of the Atmospheric Sciences*, **64**, 4127–4139, doi:10.1175/2007JAS2144.1.

Raymond, D., Ž. Fuchs, S. Gjorgjievska, and S. Sessions, 2015: Balanced dynamics and convection in the tropical troposphere. *Journal of Advances in Modeling Earth Systems*, **7 (3)**, 1093–1116, URL https://agupubs.onlinelibrary.wiley.com/doi/abs/10.1002/2015MS000467.

Reed, R. J., and E. E. Recker, 1971: Structure and properties of synoptic-scale wave disturbances in the equatorial Western Pacific. *Journal of the Atmospheric Sciences*, **28 (7)**, 1117–1133, URL https://doi.org/10.1175/1520-0469(1971)028<1117:SAPOSS>2.0.CO;2.

Rio, C., F. Hourdin, J.-Y. Grandpeix, and J.-P. Lafore, 2009: Shifting the diurnal cycle of parameterized deep convection over land. *Geophysical Research Letters*, **36 (7)**, URL http://dx.doi.org/10.1029/2008GL036779, l07809.

Rousseau-Rizzi, R., D. J. Kirshbaum, and M. K. Yau, 2017: Initiation of deep convection over an idealized mesoscale convergence line. *Journal of the Atmospheric Sciences*, **74 (3)**, 835 – 853, doi:10.1175/JAS-D-16-0221.1, URL https://journals.ametsoc.org/view/journals/atsc/74/3/jas-d-16-0221.1.xml.

Rowe, A. K., and R. A. Houze, 2015: Cloud organization and growth during the transition from suppressed to active MJO conditions. *Journal of Geophysical Research: Atmospheres*, **120 (19)**, 10,324–10,350, URL http://dx.doi.org/10.1002/2014JD022948, 2014JD022948.

Accepted for publication in *Journal of the Atmospheric Sciences*. DOI10.1175/JAS-D-20-0337.1.

Sherwood, S. C., and R. Wahrlich, 1999: Observed evolution of tropical deep convective events and their environment. *Monthly Weather Review*, **127 (8)**, 1777–1795, URL https://doi.org/10.1175/1520-0493(1999)127<1777:OEOTDC>2.0.CO;2.

Skamarock, W., J. Klemp, J. Dudhia, D. Gill, D. Barker, M. Duda, X.-Y. Huang, and W. Wang, 2008: A description of the Advanced Research WRF version 3. NCAR technical note. Tech. rep., NCAR/TN-475+STR. doi:10.5065/D68S4MVH.

Sobel, A. H., J. Nilsson, and L. M. Polvani, 2001: The weak temperature gradient approximation and balanced tropical moisture waves. *Journal of the Atmospheric Sciences*, **58 (23)**, 3650–3665, URL https://doi.org/10.1175/1520-0469(2001)058<3650:TWTGAA>2.0.CO;2.

Stephens, G. L., and Coauthors, 2010: Dreary state of precipitation in global models. *Journal of Geophysical Research: Atmospheres*, **115 (D24)**, URL http://dx.doi.org/10.1029/2010JD014532, d24211.

Stevens, B., and S. Bony, 2013: What are climate models missing? *Science*, **340 (6136)**, 1053–1054, doi:10.1126/science.1237554, URL http://www.sciencemag.org/content/340/6136/1053.short.

Stirling, A. J., and J. C. Petch, 2004: The impacts of spatial variability on the development of convection. *Quarterly Journal of the Royal Meteorological Society*, **130 (604)**, 3189–3206, URL http://dx.doi.org/10.1256/qj.03.137.

Suhas, E., and G. J. Zhang, 2014: Evaluation of trigger functions for convective parameterization schemes using observations. *Journal of Climate*, **27 (20)**, 7647–7666, URL https://doi.org/10.1175/JCLI-D-13-00718.1.

Accepted for publication in *Journal of the Atmospheric Sciences*. DOI10.1175/JAS-D-20-0337.1.

Suhas, E., and G. J. Zhang, 2015: Evaluating convective parameterization closures using cloud-resolving model simulation of tropical deep convection. *Journal of Geophysical Research: Atmospheres*, **120 (4)**, 1260–1277, URL https://agupubs.onlinelibrary.wiley.com/doi/abs/10.1002/2014JD022246.

Sui, C.-H., and Coauthors, 2020: The South China Sea two islands monsoon experiment for studying convection and subseasonal to seasonal variability. *Terr. Atmos. Ocean. Sci.*, **31**, 103–129, doi:10.3319/TAO.2019.11.29.02.

Tompkins, A. M., 2001: Organization of tropical convection in low vertical wind shears: The role of cold pools. *Journal of the Atmospheric Sciences*, **58 (13)**, 1650–1672, URL https://doi.org/10.1175/1520-0469(2001)058<1650:OOTCIL>2.0.CO;2.

Waite, M. L., and B. Khouider, 2010: The deepening of tropical convection by congestus preconditioning. *Journal of the Atmospheric Sciences*, **67 (8)**, 2601–2615, URL https://doi.org/10.1175/2010JAS3357.1.

Watson, P. A. G., H. M. Christensen, and T. N. Palmer, 2015: Does the ECMWF IFS convection parameterization with stochastic physics correctly reproduce relationships between convection and the large-scale state? *Journal of the Atmospheric Sciences*, **72 (1)**, 236–242, URL https://doi.org/10.1175/JAS-D-14-0252.1.

Weckwerth, T. M., 2000: The effect of small-scale moisture variability on thunderstorm initiation. *Monthly Weather Review*, **128 (12)**, 4017–4030, URL https://doi.org/10.1175/1520-0493(2000)129<4017:TEOSSM>2.0.CO;2.

Willett, M. R., and M. A. Whitall, 2017: A simple prognostic based convective entrainment rate for the Unified Model: description and tests. Tech. Rep. Forecasting Research Technical Report

Accepted for publication in *Journal of the Atmospheric Sciences*. DOI10.1175/JAS-D-20-0337.1.

No 617, Met Office, 53 pp. URL https://www.metoffice.gov.uk/binaries/content/assets/mohippo/pdf/library/frtr_617_2017p.pdf.

Wing, A. A., K. Emanuel, C. E. Holloway, and C. Muller, 2017: Convective self-aggregation in numerical simulations: A review. *Surveys in Geophysics*, 1–25, URL http://dx.doi.org/10.1007/s10712-017-9408-4.

Wolding, B., J. Dias, G. Kiladis, F. Ahmed, S. W. Powell, E. Maloney, and M. Branson, 2020: Interactions between Moisture and Tropical Convection. Part I: The Coevolution of Moisture and Convection. *Journal of the Atmospheric Sciences*, **77 (5)**, 1783–1799, URL https://doi.org/10.1175/JAS-D-19-0225.1.

Yano, J.-I., 2014: Formulation structure of the mass-flux convection parameterization. *Dynamics of Atmospheres and Oceans*, **67**, 1 – 28, doi:https://doi.org/10.1016/j.dynatmoce.2014.04.002.

Yano, J.-I., M. H. P. Ambaum, H. F. Dacre, and A. Manzato, 2020: A dynamical–system description of precipitation over the tropics and the midlatitudes. *Tellus A: Dynamic Meteorology and Oceanography*, **72 (1)**, 1–17, URL https://doi.org/10.1080/16000870.2020.1847939.

Yano, J.-I., M. Bister, Ž. Fuchs, L. Gerard, V. T. J. Phillips, S. Barkidija, and J.-M. Piriou, 2013: Phenomenology of convection-parameterization closure. *Atmospheric Chemistry and Physics*, **13 (8)**, 4111–4131, doi:10.5194/acp-13-4111-2013, URL http://www.atmos-chem-phys.net/13/4111/2013/.

Yano, J.-I., and R. Plant, 2012a: Finite departure from convective quasi-equilibrium: periodic cycle and discharge-recharge mechanism. *Quarterly Journal of the Royal Meteorological Society*, **138 (664)**, 626–637, URL http://dx.doi.org/10.1002/qj.957.

Accepted for publication in *Journal of the Atmospheric Sciences*. DOI10.1175/JAS-D-20-0337.1.

Yano, J.-I., and R. Plant, 2012b: Interactions between shallow and deep convection under a finite departure from convective quasi equilibrium. *Journal of the Atmospheric Sciences*, **69 (12)**, 3463–3470, URL https://doi.org/10.1175/JAS-D-12-0108.1.

Yano, J.-I., and R. S. Plant, 2012c: Convective quasi-equilibrium. *Reviews of Geophysics*, **50 (4)**, URL http://dx.doi.org/10.1029/2011RG000378, rG4004.

Yano, J.-I., and R. S. Plant, 2016: Generalized convective quasi-equilibrium principle. *Dynamics of Atmospheres and Oceans*, **73**, 10 – 33, doi:https://doi.org/10.1016/j.dynatmoce.2015.11.001.

Yano, J.-I., and R. S. Plant, 2020: Why does Arakawa and Schubert's convective quasi-equilibrium closure not work? Mathematical analysis and implications. *Journal of the Atmospheric Sciences*, **77 (4)**, 1371–1385, URL https://doi.org/10.1175/JAS-D-19-0165.1.

Zuidema, P., G. Torri, C. Muller, and A. Chandra, 2017: A survey of precipitation-induced atmospheric cold pools over oceans and their interactions with the larger-scale environment. *Surveys in Geophysics*, URL https://doi.org/10.1007/s10712-017-9447-x.

Accepted for publication in *Journal of the Atmospheric Sciences*. DOI10.1175/JAS-D-20-0337.1.

LIST OF FIGURES

Accepted for publication in *Journal of the Atmospheric Sciences*. DOI10.1175/JAS-D-20-0337.1.

Accepted for publication in *Journal of the Atmospheric Sciences*. DOI10.1175/JAS-D-20-0337.1.

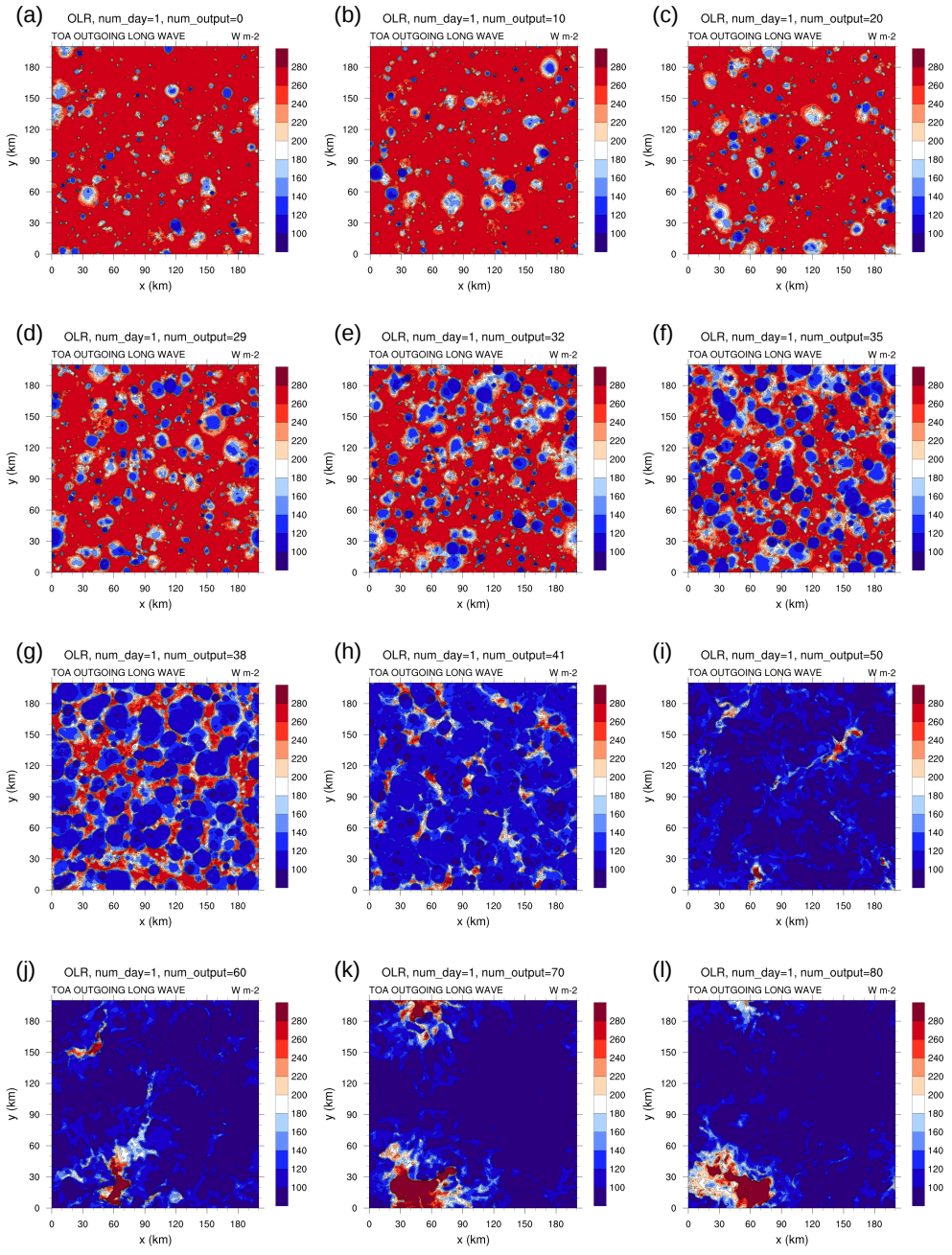

FIG. 1. Sequence of images showing the instability development in one of the four cases where convection intensified from the initial equilibrium state, under strong nudging to fix the macrostate. Colors show simulated outgoing longwave radiation. Times are (a) 0, (b) 2.5, (c) 5, (d) 7.25, (e) 8, (f) 8.75, (g) 9.5, (h) 10.25, (i) 12.5, (j) 15, (k) 17.5, and (l) 20 hours after strong nudging is initiated.

Accepted for publication in *Journal of the Atmospheric Sciences*. DOI10.1175/JAS-D-20-0337.1.

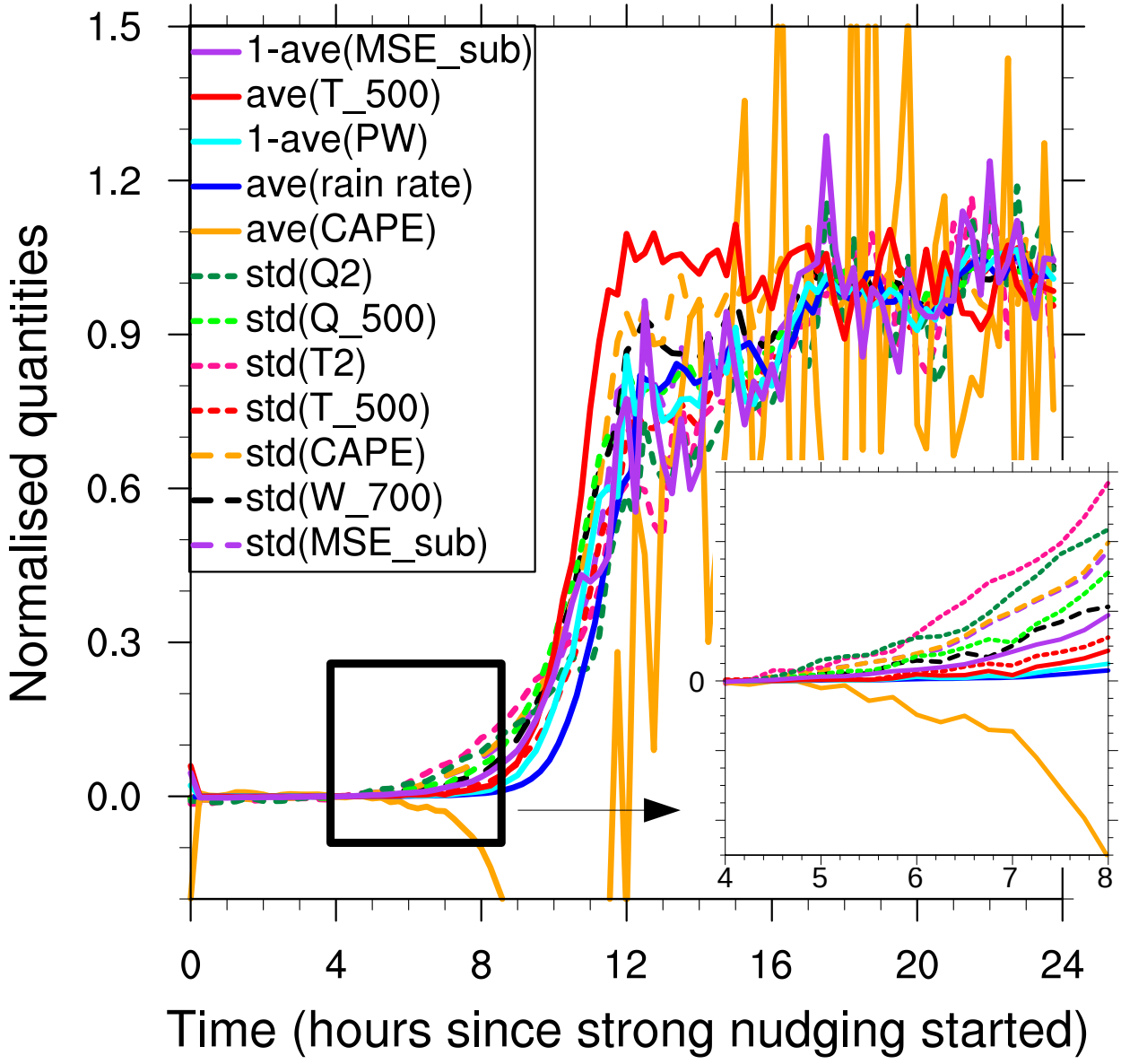

FIG. 2. Onset of unstable convective growth with fixed macrostate, in the case in Fig. 1. Horizontal axis shows time since fixing the horizontal mean (macro-)state. All quantities are horizontally averaged and shown as departures from the original state (averaged over the first few hours), normalized by the eventual departure in the final state (averaged over the last few hours), from an example numerical CRM simulation. Quantities are: Moist Static Energy (MSE) from the sub-cloud layer [varying from 346.76 to 346.28 kJ/kg], mid-tropospheric (500 hPa) temperature [from 265.33 to 265.83 K], precipitable water (PW) [from 53.88 to 52.40 mm], rain rate [from 4.6 to 2980 mm/day], CAPE [from 3273 to 3337 J/kg], and standard deviations of two-meter water vapor mixing ratio [from 0.4 to 2.4 g/kg], mid-tropospheric (500 hPa) water vapor mixing ratio [from 0.3 to 2.3 g/kg], two-meter temperature [from 0.3 to 1.9 K], mid-tropospheric (500 hPa) temperature [from 0.1 to 4.4 K], CAPE [from 287 to 2093 J/kg], vertical velocity at 700 hPa [from 0.3 to 9.8 m/s], MSE from the sub-cloud layer [from 1.0 to 7.8 kJ/kg]. Values between square brackets indicate the absolute changes from the original state (averaged over 6h) to the final state (averaged over 6h).

Accepted for publication in *Journal of the Atmospheric Sciences*. DOI 10.1175/JAS-D-20-0337.1.

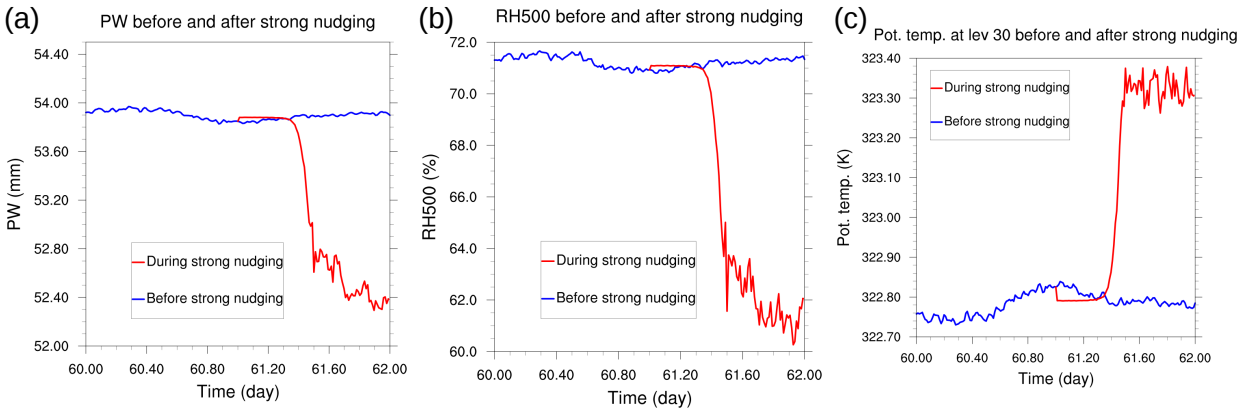

FIG. 3. Time series comparing the control simulation without strong nudging, i.e. in RCE (blue) and with strong nudging, i.e. the same unstable control simulation as Figure 1 (red). (a) Domain-mean Precipitable Water (b) Domain-mean relative humidity at 500 hPa (c) Domain-mean potential temperature at model level number 30 (about 500 hPa). The red curves only start from day 61, when strong nudging is activated. The blue curves show RCE fluctuations. The red curves show strong nudging works almost perfectly for ~10 hours, then the instability prevails and the system exponentially goes towards another state, which was not accessible from RCE fluctuations only.

Accepted for publication in *Journal of the Atmospheric Sciences*. DOI10.1175/JAS-D-20-0337.1.

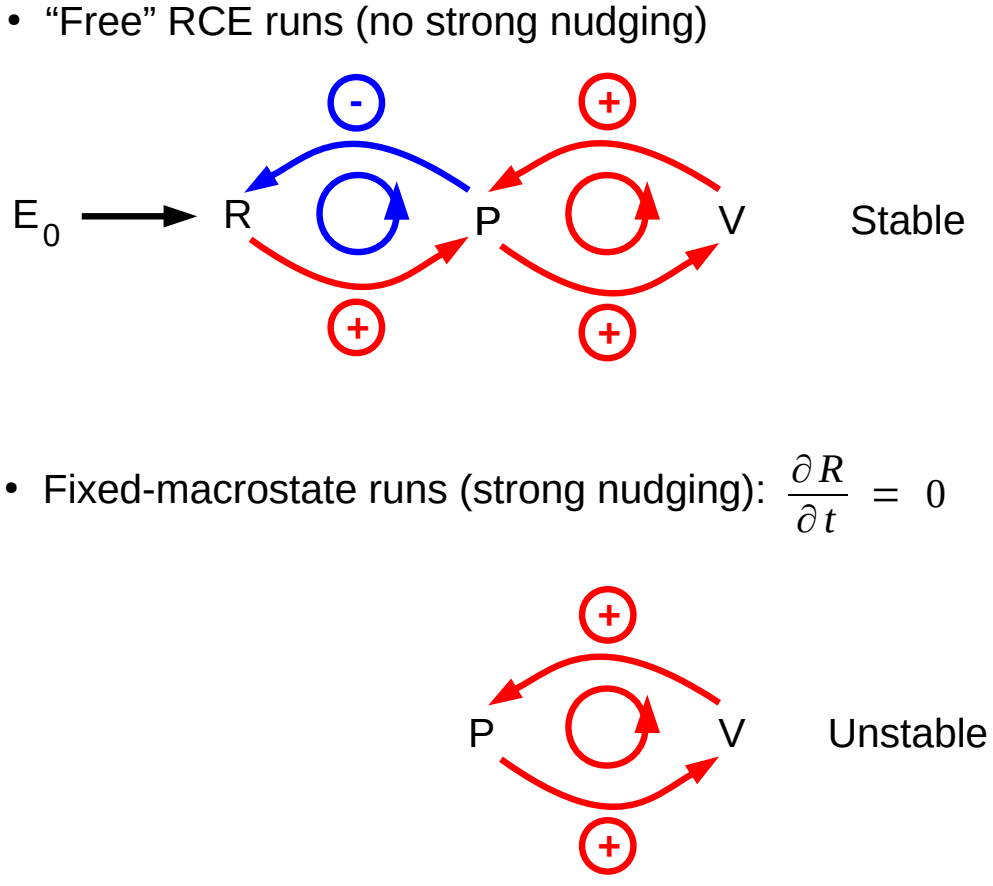

FIG. 4. Diagram showing predator-prey feedbacks in standard, interactive, “free” radiative-convective equilibrium (no strong nudging) vs. with strong nudging of the macrostate to its RCE value (non-interactive macrostate).

Accepted for publication in *Journal of the Atmospheric Sciences*. DOI10.1175/JAS-D-20-0337.1.

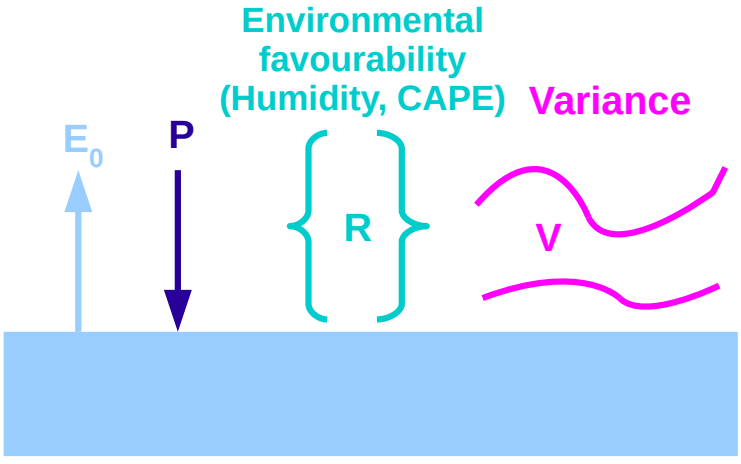

FIG. 5. Schematic of the physics behind the predator-prey model. The environmental favorability (atmospheric humidity or CAPE or others), represented by a single variable R, has a source term E_0 (evaporation or radiative cooling), and a sink term (precipitation P). The key variable in this model is the variance V, representing the microstate turbulence or microstate variability/heterogeneity/structure.

Accepted for publication in *Journal of the Atmospheric Sciences*. DOI10.1175/JAS-D-20-0337.1.

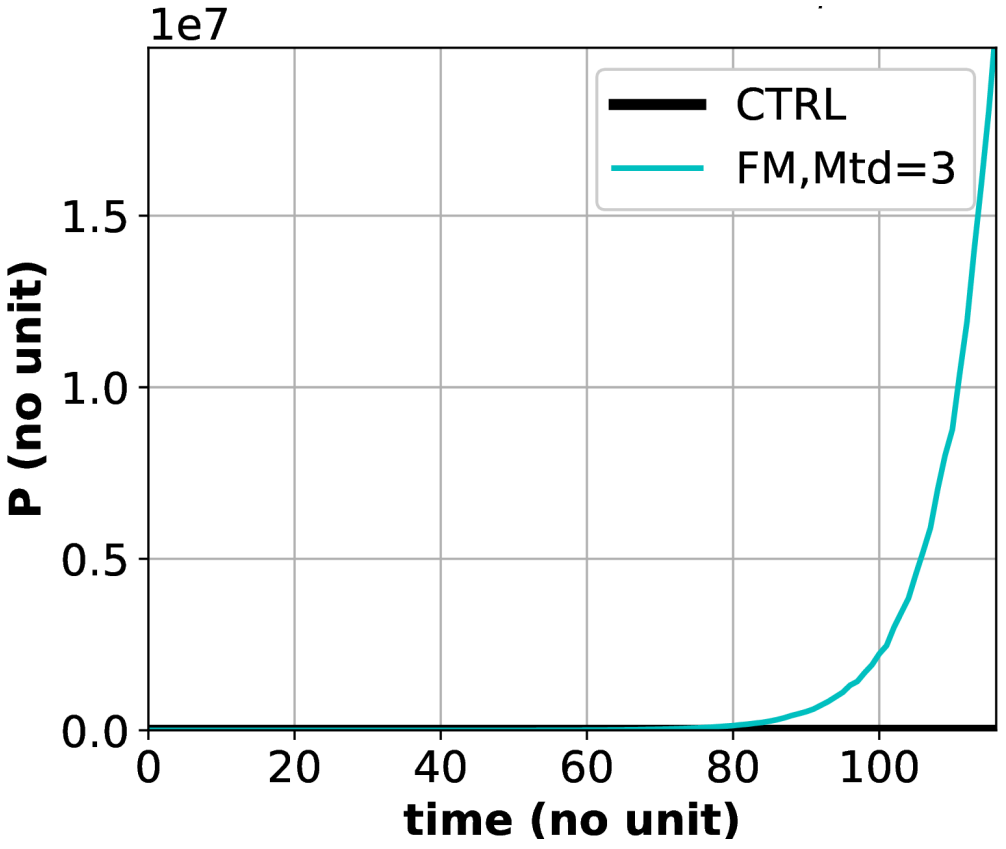

FIG. 6. Evolution of P in the Predator-Prey model, showing exponential growth of convective instability under Fixed-Macrostate conditions (FM, blue), compared to the free RCE run (black). Here $\alpha_{\text{damp}} = 0.3$ and all stochastic terms are turned off. According to our analyses, 1 time unit is approximately 12.4 min in the CRM, so the time frame amounts to 24h here.

Accepted for publication in *Journal of the Atmospheric Sciences*. DOI10.1175/JAS-D-20-0337.1.

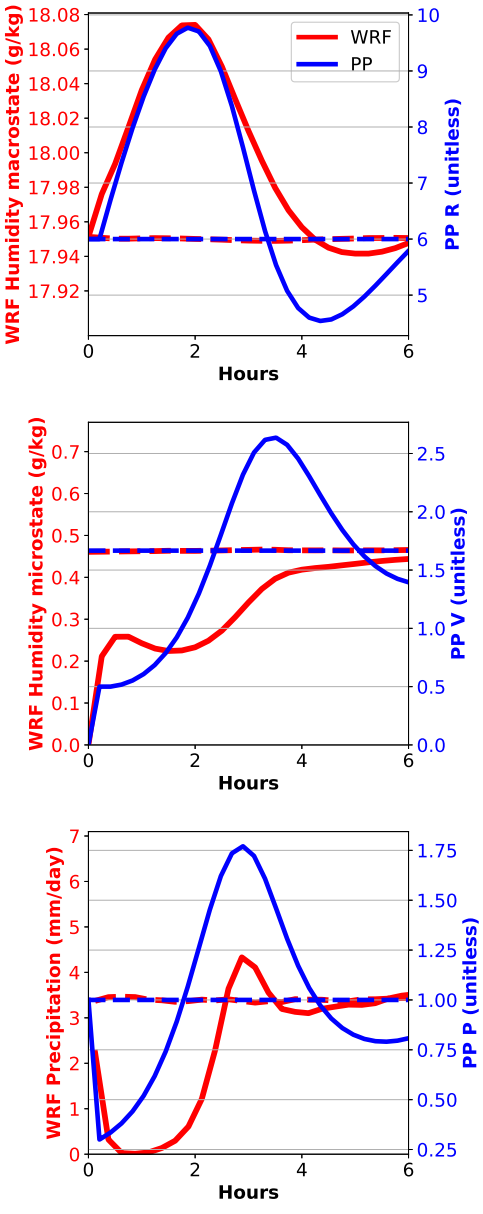

FIG. 7. Deviation and recovery of freely evolving convection following microstate homogenization. Time series are from the predator-prey model (blue) with V set to zero at time 0, vs. numerical CRM (red) predictions with microstate homogenization of temperature and humidity then restart. All stochastic terms are turned off in the predator-prey model. Panels show (Top) mean low-level (sub-cloud) water vapor mixing ratio (for the CRM) and R (for predator-prey); (Middle) standard deviation of low-level (sub-cloud) water vapor mixing ratio (for WRF) and V (for predator-prey); (Bottom) precipitation. Results are averaged over an ensemble of 19 members (for WRF) or 1000 members (for predator-prey). Dashed lines show ensemble-mean control results (no homogenization). For an optimal fit, 1 time unit in the predator-prey model is approximately 12.4 min in WRF, so that 29 time units amounts to 6h in WRF. The red line in the bottom panel is taken from Colin et al. (2019).

Accepted for publication in *Journal of the Atmospheric Sciences*. DOI10.1175/JAS-D-20-0337.1.

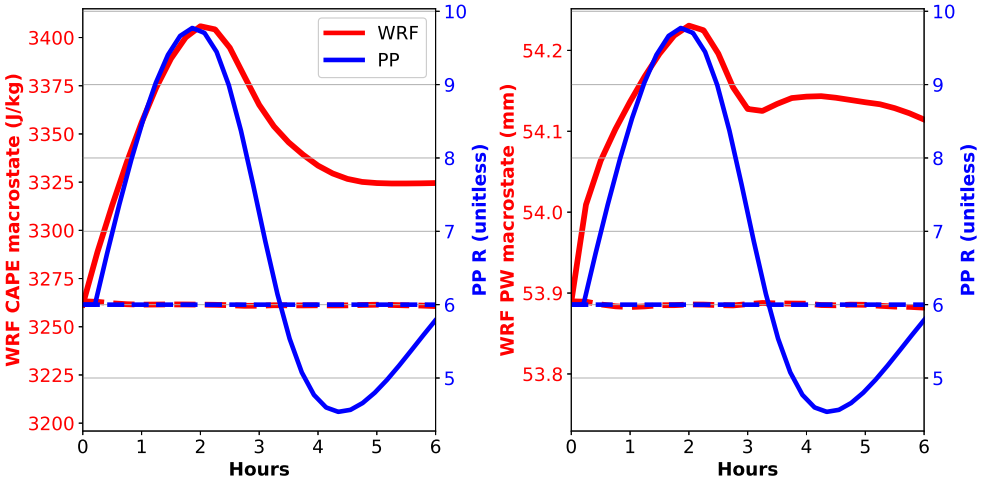

FIG. 8. As in Fig. 7a but with CAPE (left) or precipitable water (right) instead of sub-cloud humidity as R.

Accepted for publication in *Journal of the Atmospheric Sciences*. DOI10.1175/JAS-D-20-0337.1.

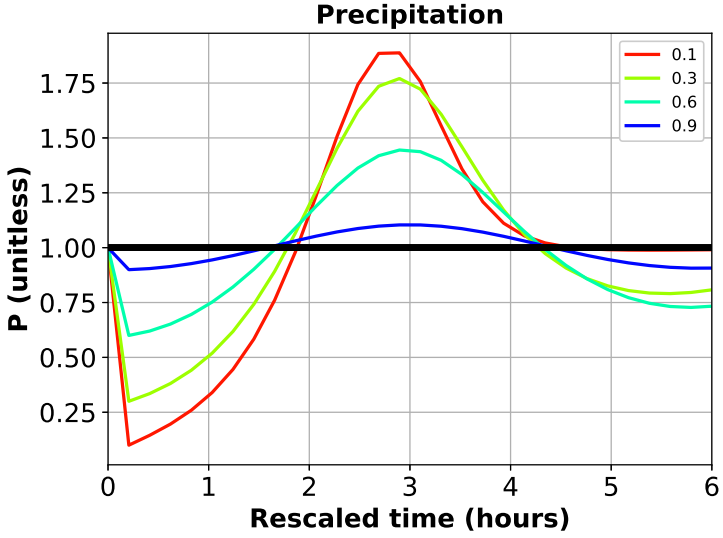

FIG. 9. Responses of Predator-Prey P as in Fig. 7c, but for different values of α_{damp} (legend, colors) and without stochastic terms. Black lines show Control (no homogenization), and colorful lines show results with homogenization (setting $V = 0$) at t=0.

Accepted for publication in *Journal of the Atmospheric Sciences*. DOI10.1175/JAS-D-20-0337.1.

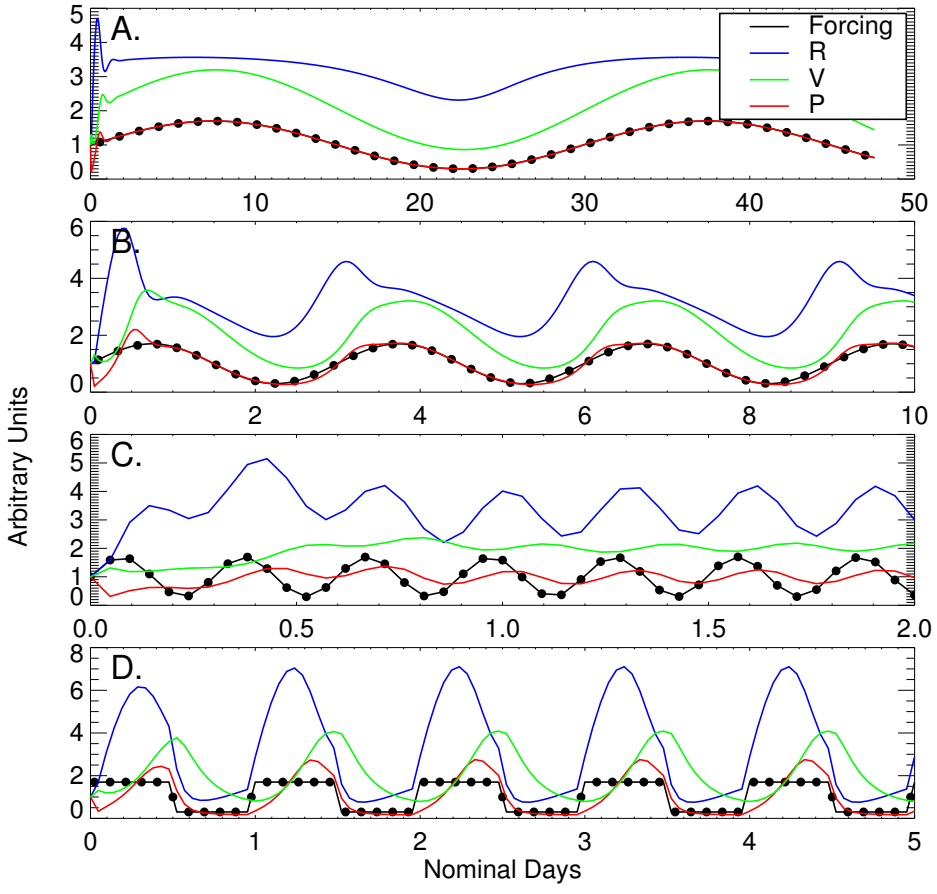

FIG. 10. Predator-prey model (original version) behavior under periodic forcing E_0 (oscillating source of $R \sim$ CAPE or humidity). In (a-c), forcing E_0 is sinusoidal at periods of (a) 30, (b) 3, and (c) 0.3 nominal days, representing respectively planetary-scale, synoptic-scale and mesoscale disturbances. In (d) forcing E_0 is on-off at a period of one nominal day, representing an idealized diurnal cycle on land.

Accepted for publication in *Journal of the Atmospheric Sciences*. DOI10.1175/JAS-D-20-0337.1.

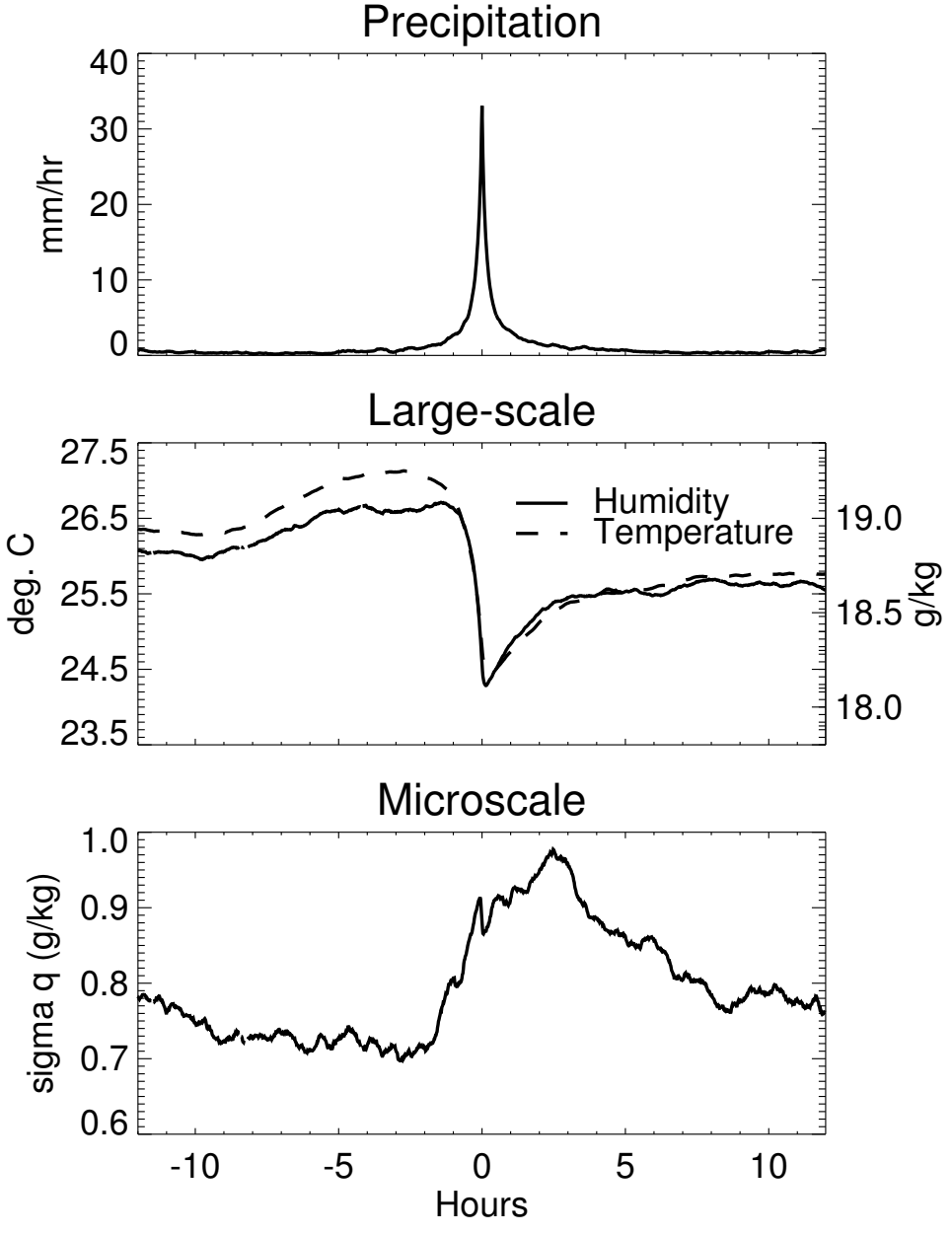

FIG. 11. Observed evolution of predator-prey variable proxies composited around rainfall peaks. Shown are (Top) mean precipitation; (Middle) mean near-surface temperature (solid) or water vapor mixing ratio (dashed), a proxy for R; and (Bottom) standard deviation of near-surface water vapor mixing ratio, a proxy for V. The x-axis shows time relative to a peak in precipitation. Data are 1-minute station data from the Manus Island ARM site, from 01 Jan 2011 through 05 July 2014.

Accepted for publication in *Journal of the Atmospheric Sciences*. DOI10.1175/JAS-D-20-0337.1.

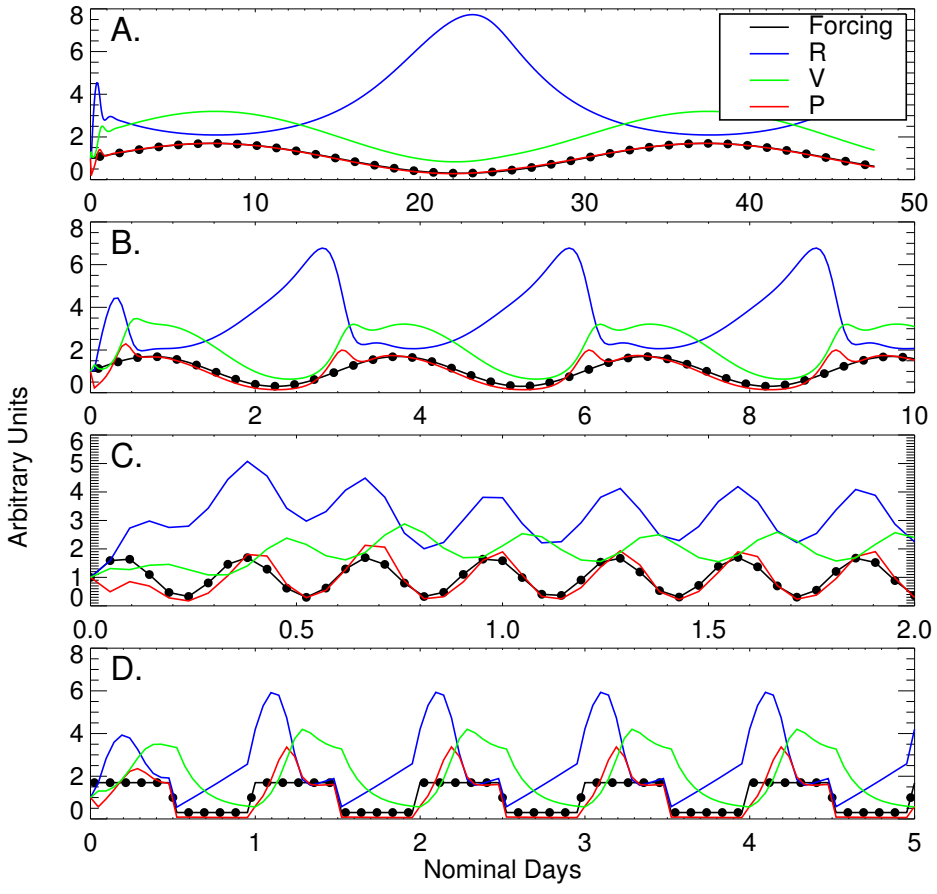

FIG. 12. As in Fig. 10 except using the Moisture Convergence version III modification of the predator-prey model, in which precipitation is influenced directly by moisture/CAPE forcing (E_0), R, and V at the same time (see Section 4). Compared with Fig 10, this shows unphysical results.

Accepted for publication in *Journal of the Atmospheric Sciences*. DOI10.1175/JAS-D-20-0337.1.